CRANFIELD UNIVERSITY
SCHOOL OF APPLIED SCIENCE

Masters By Research

Synthesis and Characterisation of Ferrofluid synthesized from Iron and Manganese.

Saadia. M. Hakim

Supervisor

Dr. Chris Sansom

Acknowledgements:

I would like to take this opportunity to thank both Dr. Chris Sansom and Dr. Paul Jones for all the help and support they have given me from when I first started this project.
I would also like to thank the most amazing husband in the world Marvin Monero for being the biggest rock a women could ever wish for; and also my parents for all the support they have given me throughout my years.

Abstract:

Ferrofluids were first used by NASA in the 1960s in order to control the motion of fluids within space, as a ferrofluid is a fluid that has unique magnetic properties. These magnetic properties allow the fluids to be applied to many different applications within various industries. Ferrofluids are not only used in more traditional methods such as within speakers but they are also being used in new industries, for examples in medical applications, due to their biocompatibility. This biocompatibility is due to ferrofluids being usually made from Iron or Manganese with a co-precipitation methodology. Ferrofluids have the unique advantage in being paramagnetic, where within a magnetic presence they would display magnetic properties and without this property the magnetism diminishes.

In this study the properties, of iron based ferrofluids are investigated and some of the key variables that define the properties of these fluids are identified.

Contents:

1.0: Introduction:

1.1: Background:

Due to the current energy climate there has been a drive to develop energy conservation and regeneration solutions for energy harvesting. Major approaches have been used to help increase “the used green” renewable energy. One of these approaches has been an increase in economical and cleaner methods of generating energy from natural resources.

A technique, which shows the potential for the recovery and conversion of low grade thermal energy, is being investigated, which also has the advantages of a lack of any moving mechanical components, uses of a magnetic liquid (Qiang Li et al, 2009).

Consider the application and production of a liquid that can be controlled by a magnetic field (Berger et al) 1999. Magnetic solids lose their magnetism above the Curie temperature, this is due to the increased thermal energy that has been supplied the electron spins becomes less aligned, the domain walls also tends to rearrange so that the large scale field energy is reduced by pointing at different directions the material at this point loses its magnetisation. Due to this creating a strong magnetic liquid is not as easy as producing a strong magnetic solid. The thermal energy also overwhelms the tendency of the electrons to align in magnetic domains. Ferrofluids, which are colloidal suspensions of magnetic material in a carrier fluid is an example of a liquid that responds to an external magnetic field. The coupling of liquid and magnetic behaviour, due to their unique magnetic nano-particles with dimensions in the order of 50nm means that the liquids location may be manipulated by an applied magnetic field (Qiang et al, 2009).

Stephen Pappell in the 1960’s of NASA first developed ferrofluids as a method of controlling fluids in space. NASA initially used them as rotating shaft seals in satellites, and they now serve the same purpose in a wide variety of machines, ranging from centrifuges to computer hard disk drives (Berger et al, 1999).

A Ferrofluid is a colloidal suspension of ferromagnetic particles in a carrier fluid. The ferromagnetic particles are magnetic in nature. Research is taking place that is aimed at producing thermal regeneration solutions for various industrial sectors. Devices are being developed that use the flow and the rheological properties of ferrofluids that is used for thermal pumping and refrigeration. According to (Wurfel et al, 2009) the current maximum efficiency for a typical solar cell is within the region of 12 to 42%. The process hopes to have a significant improvement on the low grade energy solutions by increasing the energy conversion efficiency between ranges of 25 to 30%.

The aim of such a device would be to provide cost reductions by significant cooling in high thermal loss appliances for example computer drives and trying to re-use the energy harvested from the system. Examples of applications for this project would be the cooling of server hubs in large data centres, and the extraction of waste heat from powered machine tools, such as grinding machines.

For this investigation, a Ferrofluid is needed that enables optimum performance of cooling in such a device. This research will focus on synthesising Ferrofluid made from Iron and Manganese in order to obtain a repeatable process.

1.2: Aims & Objective:

Aim:

The aim of this project is to synthesise and characterise ferrofluids under different conditions in order to investigate the repeatability and consistency of the process.

To achieve this aim, the following objectives will need to be met.

1. Prepare Ferrofluids using variations around a standard process, and characterise the Ferrofluids.
2. Develop a method to measure the Curie temperature of the ferrofluids.
3. Compare the different ferrofluids synthesised during this study
4. Compare the preparation methods, investigate the variability in the process, and select the preferred process for our energy harvesting application.

2.0: Literature Review:

2.1: Ferrofluids:

Ferrofluid are fluids that exhibit magnetic behaviour. They consist of a colloidal suspension of super-paramagnetic particles (ferromagnetic or paramagnetic) in a carrier fluid. The fluid itself is magnetic due to the magnetic nature of suspended particles, which are usually ferrous in composition and nanometre in dimension (~10nm). In order, for the magnetite to remain in suspension the particle diameter should be in the order of 10nm. At room temperature, the thermal energy of these colloidal particles is of the same magnitude as the gravitational and magnetic attraction, ~4 x 10^{-21} J, and therefore the particles remain suspended (Berger et al). Ferrofluids tend to be stable in nature, where the solid particles should not agglomerate or phase separate even if a strong magnetic field is present. The particles do not degrade over time. The nano structure of the particles, and thermal agitation, allows them to be dispersed evenly in a solution. The nano particles are stabilised in the carrier liquid as they tend to agglomerate due to the Van der Waals forces. Ferrofluids are also susceptible to air oxidation, in order to prevent air oxidation and agglomeration the magnetic particles are coated with a surfactant (Maity et al 2007). A typical composition of a ferrofluid is approximately 5% magnetic solids, 10% surfactant and 85% carrier, by volume.

Ferrofluids can be seen to express the magnetorheological behaviour. The magnetorheological behaviour is found in Ferrofluids as they are able to change their fluidic properties, in particular viscosity under a magnetic field. This fluidic property can be changed due to the combination of carrier fluid and the suspended magnetic particles.

The particle compositions of the ferrofluids that are considered in this report are composed of spinel ferrites. The ferrites have the composition structure AB_2O_3 where A and B are the metal cations in the composition, in this case Iron (II) and Iron (III). The Oxygen ions that are within the composition are close cubic packed (FCC) and they have two different interstitial sites, this is where the cations are bonded. The two different interstitial sites may be either tetrahedral or octahedral. The A cations (Iron (III)) occupies one eighth of the tetrahedral holes and B (Iron (II)) cations occupies a quarter of the octahedral holes (Berger et al, 1999). The tetrahedral sites are where the cation is surrounded by four Oxygen ions and the Octahedral is when the cation is surrounded by six Oxygen ions.

The cations in question are usually transitional metal cations, which could be either: Fe, Mn, Cu, Zn, Co or Ni. The transition metals have unpaired electrons and they possess a

net magnetic moment that interacts internally to generate a state of magnetic ordering. The properties of the ferrite will change if the combination of the transition metals are altered; such as the net magnetic ordering, the size of the particles and the Curie temperature. An example of this is $MnZnFe_2O_4$, where Zn is a non-magnetic ion that occupies the tetrahedral interstitial site that is within the cubic structure, increasing the total net magnetic moment (Kools and van der Valk, 2004).

As, mentioned before the size of the particles tends to be in the size of nanometers. This is usually dependent upon the medium used, and to how much substitution the transition metal has in the structure during the co-precipitation stage that occurs during the synthesis of the ferrofluid. Various mediums can be used as the co-precipitation base, such as: NaOH, NH_3 and CH_3NH_2. The co-precipitation is the synthesis that is generally preferred; other methods can also be utilised such as ball milling and wet chemical synthesis via reverse micelles. (Morrison et al, 2003).

The magnetic behaviour of ferrofluids is exhibited due to their long range ordering that occurs at an atomic level. This is where unpaired electrons spin line up in what is known as a domain. When the Ferromagnetic particles are sized in the order of nanometers, and are in colloidal suspended ferrofluids, they continually exhibit a fixed dipole magnetic field since they are magnetically singly domained. (Odenbach,2002).

When heated above the Curie temperature it can be seen that the intrinsically magnetic materials lose some of their magnetic properties, mainly their magnetisation (magnetic moment/volume). In the case of magnetite when the fluid is heated above its Curie temperature the magnetic property of the nanoparticles will change from being ferrimagnetic to being paramagnetic i.e. showing no magnetic order and is only affected by an external magnetic field. This is related directly to the magnetic field strength that is produced and the transition occurs due to a disruption in the long range ordering of the material. According to Odenbach, 2002, the Curie temperature in ferromagnetic materials is below the melting point.

The magnetisation and the Curie temperature of all ferromagnetic materials are based on the composition of the materials. The Curie temperature of the fluid can be tailored for each individual need as the chemical composition can be changed and when the particles are added in a Ferrofluid suspension due to the single domain nature of the solid and the interaction of the particles and the carrier fluids.

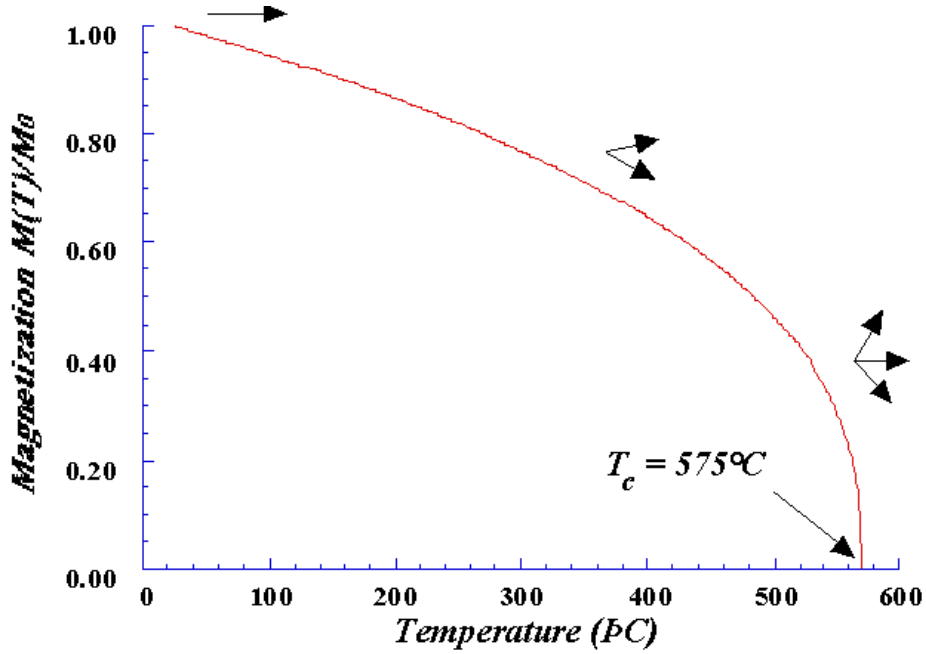

Figure 1: Graph showing the Curie temperature for Magnetite by comparing the temperature and magnetization (Moskowitz.B, 1991).

As discussed previously, due to Van der Waals forces agglomeration is not prevented; in order to maintain the stable nature of the fluid the magnetic particles needs to be coated with a surfactant. An example of a surfactant is Oleic Acid, which is a long chain molecules with a thickness between 2-3nm. The surfactant is chosen so that the dielectric properties match that of the carrier fluid (Odenbach, 2003). The hydrodynamic behaviour of the innate ferrous nano-particles is also affected by the surfactant. The lifespan of the fluid can also be dictated by the surfactant as the surfactant over time can break down due to chemical degradation and particle interaction. Ferrofluids that are prepared from uncoated particles can be seen to have unstable surface deformations when a magnetic field is applied. (Déry et al, 2008).

The viscosity of the fluid has an impact upon fluid flow. The carrier fluid primarily governs the physical properties of the fluid as it is the most dominant component (Moskowitz et al, 1995). The carrier fluid is usually an organic solvent or a hydrocarbon; but can also be an inorganic solvent. The selection of the carrier fluid is usually determined by the desired properties of the ferrofluid in a given application. The service temperature of the ferrofluid also needs to be considered, since fluid will need to be heated to a certain temperature without degradation occurring. In order for the Curie temperature to be approached it will need to be lower than the flash point of the carrier fluid in order to avoid any unwanted reaction.

The particle density and the carrier fluid mix play a large part on the magnetisation and base viscosity of the fluid and it is important to consider both for the applications. The overall magnetic and rheological properties are determined by the particles, surfactant and the carrier fluid.

The main polar carrier fluid for a magnetic fluid is water. Water based ferrofluids are considered to be a special category of polar ferrofluid concentrating on the particle interactions and the agglomerate formation. Water based Ferrofluid are very important within the biomedical field such as magnetic cell separation, due to their biocompatibilty properties and their colloidal stability.

Ferrofluids are usually defined by their magnetisation strength in Gauss (G) and their viscosity in centiPose (cP) together with a quoted surfactant and carrier fluid.

Commercially available ferrofluids are usually based on Magnetite; an Iron formulated particles (Fe_2O_3) and is produced for applications in loudspeakers. For wide scale use and for the application of cooling and conversion as discussed, fluids will need to be prepared that are tailored for their specific applications by tailoring at the Curie temperature, viscosity and magnetisation (Berger et al, 1999).

2.2: Magnetic behaviour of Ferrofluid

One of the properties of a ferrofluid is its magnetic property. Magnetism comprises a very distinctive dipole orientation, with the two poles separated by a finite distance. Many atoms have permanent magnetic moments due to the magnetic dipoles that are present. The orientation of atomic moments within the assembly is usually random, which is the reason why the net magnetic moment is generally zero. The magnetic field is produced by the orbital motion of electrons around the nucleus and the spinning motion around their own axes.

According to a materials magnetic behaviour a material can be classified either ferromagnetic, antiferromagnetic, ferrimagnetic, paramagnetic or diamagnetic.

Ferromagnetic materials have a dipolar interaction that has parallel alignment of dipoles. This may result in a material having a net magnetisation even with an absence of an external field. Ferromagnets have great engineering importance due to the large magnetic fields that can be retained or eliminated. Examples of ferromagnetic materials include Iron, Cobalt, Nickel and rare earth materials such as gadolinium. (See figure 2)

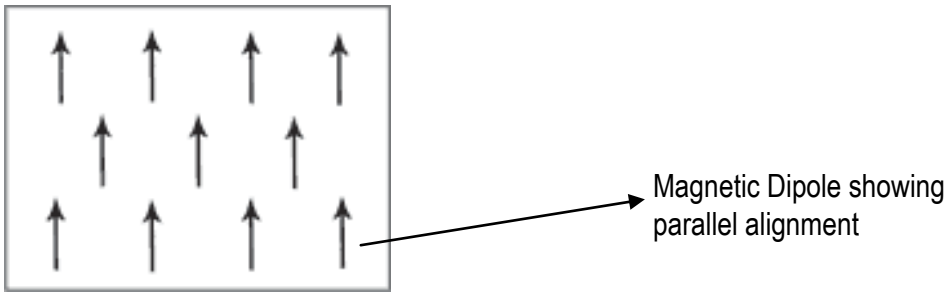

Figure 2: Diagram showing the magnetic dipoles that is present in Ferromagnetism

Anti-ferromagnetic materials do not show any magnetism even when in the presence of an external magnetic field. The dipoles of these materials are aligned in a regular pattern with the neighbouring spins that are on different sublattices pointing in opposite directions. Examples of anti-ferromagnetism are found in Manganese and Chromium in a solid state and at room temperature. (See figure 3a)

The dipoles of ferrimagnetic materials of adjacent atoms align in opposite directions. The number of moments pointing in one direction is different from the ones pointing in opposite directions, therefore creating a considerable net magnetisation the absence of a magnetic field. Generally ferrimagnetic materials have a lower magnetisation compared to

ferromagnetic materials, this is due the effect of the opposed dipole moments. Magnetite and ferrite are ferrimagnetic materials. (See figure 3b)

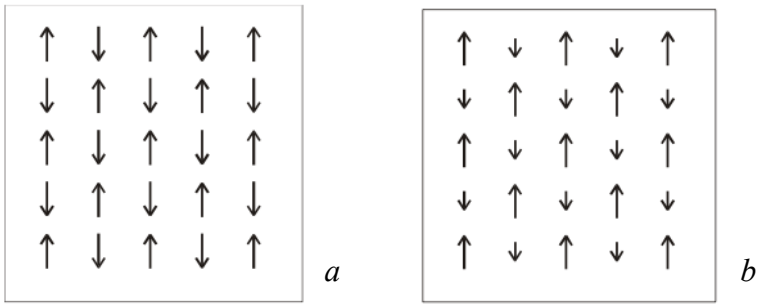

Figure 3: Diagram indicating antiferromagnetic (a) and ferrimagnetism (b).

Paramagnetic behaviour is shown by materials when the atomic moments align under the presence of a magnetic field, and where some of the atoms and ions in the material have a net magnetic moment due to unpaired electrons in partially filled orbitals. The magnetic effect is small and therefore disappears when the magnetic field is removed; when a magnetic field is present a partial alignment of the atomic magnetic moments in the direction of the magnetic field can be seen. This results in a net positive magnetisation and positive susceptibility. (Mokowitz.B, 1991). An example of this is found in aluminium, platinum, calcium and sodium.

Diamagnetic materials behave in a similar manner to paramagnetic materials, the main difference being the atoms align opposite to the applied field. This is due to the orbiting electrons exhibiting non-cooperative behaviour in the presence of a magnetic field (Mokowitz, 1991) producing a very small negative magnetic effect. The atoms do not have any magnetic moments, due to the orbitals shells being filled. Examples are Copper, gold, silver. (see figure 4)

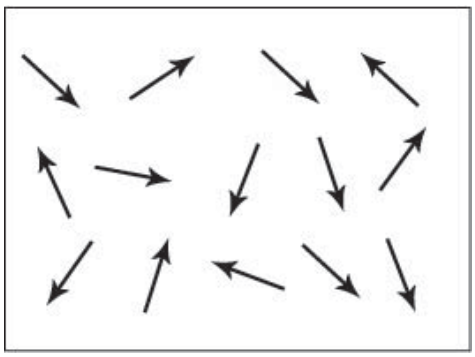

Figure 4: Diagram indicating Paramagnetic and Diamagnetism under a magnetic field.

Domains are where a magnetic material have small volume regions. Individual magnetic moments of neighbouring atoms are oriented and aligned with one another in the same direction. The field energy within a material is minimised by domains. Within a ferromagnetic material a single domain has the highest potential energy. If the single domain was divided into two, the external magnetic field is reduced and will continue to reduce as the single domain is further divided. Adjacent magnetic domains have a boundary called the domain wall. The direction of the magnetic moment in the neighbouring domain can be conducted through this. The domain wall is usually 100 atoms wide. The domain wall is created by the magnetocrystalline anisotropy energy and the exchange energy. The width of the domain wall is due to the two opposing energies both of which are as low as possible in order for the two states to be in a more favourable energetic state.. The interactions among the atomic moment are associated with the exchange energy, and this is minimised when the difference between the dipoles becomes smaller. The magnetic moments align in a certain direction due to crystal symmetry and stress. This is associated with the magnetocrystalline anisotropy and it increases as the domain wall becomes wider. The width of the domain wall is reduced when the anisotropy energy is low and the crystal lattice axes are aligned to the magnetic moment. Magneto-crystalline anisotropy energy is necessary to deflect the magnetic moment in a single crystal from the simple magnetisation direction to a more complex one. When the sum of the exchange and the magneto-crystalline anisotropy is at a minimum, the equilibrium domain wall width will be reached.

A domain wall that is considered ideal would be independent of position. Due to crystallographic defects such as foreign oxides, atoms ad insulators, this is not always the case. This will prevent the formation of domain walls and in order to overcome this, greater magnetic field needs to be applied (Moskowitz. B. 1991).

A demagnetised ferromagnetic material will become magnetised in the presence of a magnetic field, this is because ferromagnets can retain a memory of an applied field once it is removed. This behaviour is known as hysteresis, a graph representing this behaviour is known as the hysteresis loop. The graph shows the variation of magnetization with magnetic field. (B. Moskowitz, 1991). This will happen first by a domain growth whose moments are closely aligned to the applied field. Domain rotation towards the direction of the applied field occurs when the domain growth finishes. The material remains magnetised when the applied magnetic field is removed; some magnetisation is lost because the domains tend to rotate back to their original position.

The temperature also has a big effect on magnetisation. Thermal oscillation completes the magnetic dipoles when the temperature increases to enable the dipoles to position themselves in a specific way. The material becomes paramagnetic when the temperature rises beyond a certain point (Curie temperature) and the material can no longer maintain its intrinsic domain formation. This is because at the Curie temperature (Tc) even though the electronic exchange forces in ferromagnets are large, thermal energy overcomes the exchange and produces a randomising effect. Above the Curie temperature the ferromagnets appear disordered and below the Curie temperature the ferromagnets appear ordered. The saturation magnetisation at the Curie temperature is at zero.

As, mentioned previously the Curie temperature is defined as when the ferromagnetic behaviour is lost and the material starts to behave as a paramagnetic material. (See figure 5)

Material	*Curie Temperature (K)*
Iron (Fe)	*1,043*
Cobalt (Co)	*1,394*
Nickel (Ni)	*631*
Gadolinium (Gd)	*293*
Magnetite	*858*

Figure 5 Table showing the Curie Temperatures of common magnetic materials

The Curie temperature follows the Curie-Weiss law:

$x = C / T - T_c$

The Curie-Weiss law describes the magnetic susceptibility (x) of a ferromagnet in the paramagnetic region above the Curie Point:

C is the material specific Curie constant and T_c is the absolute temperature, measured in kelvin. The amount of energy that is needed to break up the domain long range ordering in the material is told by the Curie temperature. Spontaneous magnetisation occurs below the Curie temperature.

The Curie temperature can be obtained from a domain magnetisation versus temperature curve to the value that intercepts the temperature axis. An accurate method to determine

the Curie temperature is to find the point of maximum curvature from the domain versus temperature curve. If the measured data is differentiated twice, the maximum value from the second derivative corresponds to the maximum curvature point and this gives a better estimate of the Curie temperature.

The Néel temperature like the Curie temperature is a characteristic of the material, and marks the transition from the antiferromagnetic to paramagnetic behaviour. This means, that the thermal energy within the material becomes large enough to destroy the macroscopic magnetic ordering. The Néel temperature is analogous to the Curie temperature.

The nano-particles in a ferrofluid, because of their size, have a single magnetic domain with either ferromagnetic or ferrimagnetic behaviour in the molecular scale. Nano-magnetite also has a larger initial susceptibility than micro-magnetite, the coercive field and remanence is also larger for the former than for the latter. This is due to that majority of nano-magnetite consists of singly domained particles. The particles could also be paramagnetic due to zero coercivity and remanence in the colloidal scale; this behaviour is known as super-paramagnetic as it is similar to paramagnetic but with a much larger magnetisation. Zero coercivity of a ferromagnetic material is the intensity of the applied magnetic field that is required to reduce the magnetisation of the material to zero, this occurs after the magnetisation of the sample is at saturation. Therefore the coercivity measures the resistance of a ferromagnetic material becoming demagnetized. After an external magnetic field is removed from a ferromagnetic material remenance is the magnetization that is left behind (Viota. L. J, 2007).

2.3: Crystallography

The unpaired electrons of magnetite (Fe_2O_3) enables the ferrofluid to the have the magnetic properties that are so highly desired. Magnetite particles crystallise in the form of an inverse spinel structure above 120 K, where the oxide ions are within a close packed arrangement. The iron (III) ions are equally occupied between a 1/4 of the octahedral space and a 1/8 of the tetrahedral space, whilst the iron (II) ions are occupied within the whole octahedral space. Electron spins of iron (III) ions in octahedral holes are aligned antiparallel to those in tetrahedral holes; therefore, no net magnetisation is observed from these ions (Berger et al, 1999). The iron (III) ion spins and the iron (II) ions spins are aligned parallel in adjacent octahedral sites. This leads to a net magnetisation. The antiparallel spins that are held throughout the solid, and do not cancel, are known as ferrimagnetism. As, was discussed earlier ferrofluids are actually paramagnetic or super paramagnetic, this means that the ferrofluid is able to de-magnetise more rapidly compared to its counterparts (ferrimagnetic or ferromagnetic solid) even though it is able to react to a magnet in the same manner. The de-magnetisation occurs more rapidly within a ferrofluid because the magnetic domains are the same size as the actual particles. Manganese and cobalt ferrites, $MnFe_2O_4$ and $CoFe_2O_4$, respectively, also have the inverse spinel structure and have been used in the preparation of ferrofluids (Berger et al, 1999). The cubic centre unit cells layer sequence and that for a tetragonal unit cell are shown in Figures 6-7 below:

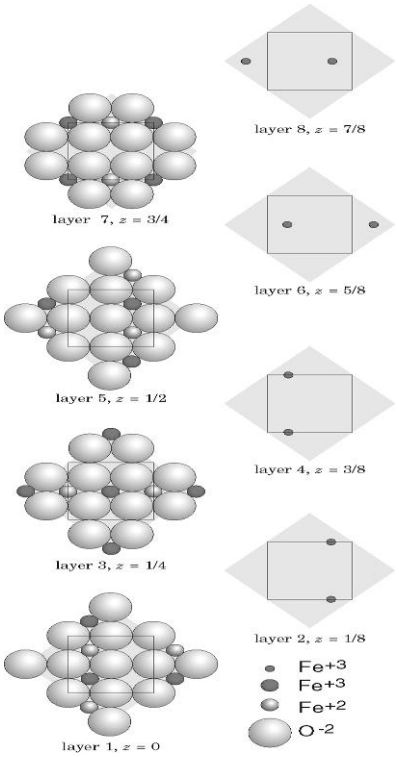

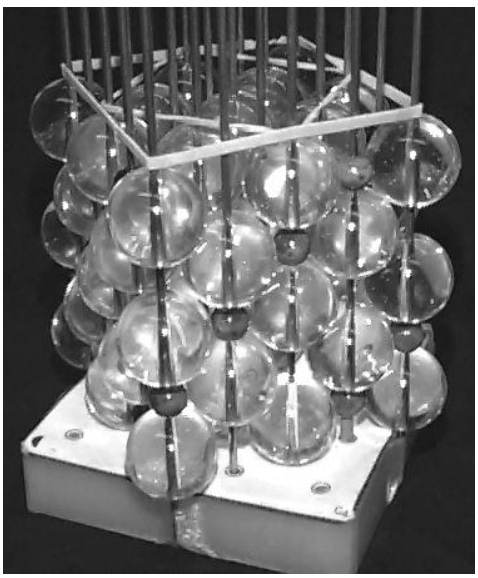

Figure 6: The cubic unit cells layer (Berger et al). *Figure 7:* A cubic unit cell built with a kit (Berger et al).

2.4: Different Experimental methods of preparing ferrofluids, magnetic characterisation and carrier Fluids from literature:

A method of preparing ferrofluid, reported by R. Arulmurugan et al (2006), was via the chemical co precipitation method of the perpetration of fine particles of $Mn_{1-x}ZnxFe_2O_4$ (with the x varying from 0.1 to 0.5.).

A solution of NaOH (0.64M dissolved in 1300ml water) was heated until it reached the boiling temperature. The $MnCl_2$, $ZnSO_4$ and $FeCl_3$ in their respective stoichiometry were mixed with the NaOH and kept at 801°C. The pH was thus adjusted to approximately 12, within 10 s under constant stirring. Positive particles were neutralised by the addition of sodium hydroxide (NaOH = 0.6M). This treatment had an important effect upon the particle size distribution, which is shifted to larger hydrodynamic diameters and significantly broadened, suggesting increased aggregation. This observation is due to the particle suspension being primarily stabilised by electrostatic repulsion and the absorption of hydroxide on the surface of the particles (Déry et al. 2008).

The molar ratio of Me^{2+} ions and Fe^{3+} ions, initially taken for different values of partial substitution of zinc and manganese was 0.5. The precipitation and formation of nano-ferrites takes place by the conversion of metal salts into hydroxides, this occurs immediately and is followed by the transformation of hydroxides into ferrites.

For the transformation of hydroxides into spinel ferrites a temperature of 951°C for one hour duration was sufficient. Dehydration and atomic rearrangement is involved in the conversion of the intermediate hydroxide phase into ferrite.

Fine particles were characterised at this stage, by collecting a sufficient number of particles using magnetic separation. The particles were then washed several times with water, followed by acetone, and then dried at room temperature.

The coating of the surfactants takes place between the pH levels of 10 and 11; therefore the pH of the remaining solution was reduced to ≈10. The Sodium Oleate solution was prepared by slightly heating the surfactant (oleic acid) with NaOH at a pH level of 10. This was then transferred to the reaction vessel and stirred for two hours. Coating of the surfactant was carried out at a time of 30 minutes. Using dilute HNO_3 decantation had been conducted. To remove any soluble impurities the product was washed several times with distilled water. The excess water was then removed by acetone washing; the coated particles were dispersed in heptane and centrifuged at 5000 rpm for two hours.

This preparation method was not considered to be the best method for the preparation of the ferrofluid in this instance as too much excessive Sodium Oleate was produced owing to the evaporation of the aqueous solution.

Martinez-Mera et al (2007) also synthesised the magnetite nano-particles similar to that of Arumurugan. Oleic acid was produced to act as the surfactant to the ferrous nano-particles, and a 1M solution of sodium oleate was formed for the oleic acid. This was achieved by mixing a 3M solution of NaOH to 0.5M of oleic acid, conducted at 40˚C, and stirred for 30mins. The sodium oleate was added to the reaction chamber and was further stirred until the temperature of 80˚C had been reached.

From both the two methods it was concluded in the literature, that both evaporation of the liquid and agglomeration were the problem that was the most common. Due to this, a new method was developed that combined both of the methods mentioned earlier to see if this would reduce the level of agglomeration and evaporation of the liquid.

The method that is described is of co-precipitation: 150ml of 4M solution of NH_4OH being produced. 10ml was retained for future use, and the remaining NH_4OH was poured into the reaction vessel and heated between 60 to 80˚C. The stirrer was then turned on low speed and 25ml solution of 0.5M of $FeCl_3 \bullet 6H_2O$ and $FeCl_4 \bullet 4H_2O$ was prepared and left for 15 minutes. The oleic solution was prepared with the retained NH_4OH and was combined with 1M oleic acid. The solution was then added to the reaction vessel and was left to stir for an extra 15 minutes. The magnetite was then separated from the solution by holding a magnet under the reaction vessel and pouring out the liquid. It was then rinsed with distilled water and separated with the magnet and was repeated if necessary. Preparation of the ferrofluid at different temperatures was also observed, 80˚C considered to be the optimum. At lower temperatures i.e. between 20 to 45˚C a large amount of agglomerationn was noted.

Zins et al (2005) presented a method to synthesise and characterise aqueous Magnetic Nickel-Zinc Ferrite fluids. Aqueous mixtures of the metallic salts ($NiCl_2$, $ZnCl_2$ and $FeCl_3$) were co precipitated in an alkaline medium (NaOH) in order to prepare the particles. The NaOH was boiled to a temperature of approximately 80ºC and the metallic salts were added to it. Vigorous stirring and constant heat were applied for 90 minutes. The magnetic nano-particles were washed with distilled water and then dispersed in Nitric Acid with a concentration of 2Mol/L. The particles were left for 15 minutes under vigorous stirring. This method creates positive surface charges but not enough for the ferrofluid to stay stable in time. The particles were then mixed in a boiling solution of aqueous nitrate mixture ($Fe(NO_3)_3$, $Ni(NO_3)_2$ and $(Zn(NO_3)_2$. This was left for 30 minutes, the end

precipitate was then washed again with nitric acid of the same concentration and then twice with acetone. 50ml of water was used to disperse the particles fully and they were then centrifuged, the end supernatant being the finished ferrofluid.

Ferrofluids that are made from Mn-Zn ferrite nano-particles are one of the biggest contenders for heat transfer applications, whose magnetisation is dependent upon temperature. When it is heated in a non-uniform magnetic field; due to the inhomogeneous distribution of fluid density in a temperature gradient, the magnetic convection and natural convection is influenced. The adiabatic magnetisation causes a considerable change in fluid temperature when the fluid is close to the Curie temperature. The Curie temperature is reduced to the operating range by using the Mn-Zn Particles. There has been the development of a variety of solution based synthesis techniques but the preparation of Mn-Zn particles with desirable size and magnetic properties is still a challenge. This is due to problems in maintaining the stoichiometry and ensuring the chemical homogeneity.

Arulmurugan et al (2006) describes a method using chemical co-precipitation. Fine particles of $Mn_{1-x}Zn_xFe_2O_4$ with the x varying from 0.1 to 0.5 where prepared via chemical co-precipitation. Aqueous solutions of $MnCl_2$, $ZnCl_2$ and $FeCl_3$ were mixed in their respective stoichiometry and thus kept at 80ºC. This was then added to a boiling solution of NaOH (0.64M dissolved in 1300ml of distilled water). The pH was adjusted to 12 and stirred for 10s. The molar ratio of Me^{2+} ions and Fe^{3+} ions, initially taken for different values of partial substitution of Zinc with Manganese, was 0.5. In the reaction vessel the final solution is adjusted so that $[M/OH^-]$ ratio is ≈0.2 ($M= Mn^{2+} + Zn^{2+} + Fe^{3+} = 0.15$ mol^{-1}). Conversion of metal salts into hydroxides occurs immediately, which is then followed by the transformation of hydroxides into ferrites therefore forming and precipitating nano ferrites. The transformation of hydroxides into spinel ferrites was conducted at a temperature of 95ºC for the duration of one hour. This transformation of the intermediate hydroxide stage into the Ferrite stage occurs due to the atomic rearrangement. Magnetic separation was thus used to separate the ferrite particles which were then characterised. This was achieved by the particles being washed several times with distilled water, followed by acetone and then dried at room temperature. The coating of the surfactant takes place only at a pH that is between 10 and 11, therefore the pH of the remaining solution was reduced to ≈10. The surfactant that was used was sodium oleate solution which was synthesised by slightly heating the oleic acid with NaOH solution at a pH of 10, which was then added to the reaction vessel and left for a further 2 hours. This coating of the particles was conducted at a temperature of 80ºC, maintained for 30 minutes.

Decantation was then conducted using dilute HNO_3. The end product was washed with distilled water twice in order to get rid of any soluble impurities. The excess water was then washed with acetone. The coated particles were dispersed in heptane and centrifuged at 5000rpm for 2 hours.

Two preparation procedures were presented by Vekas et al (2000); one was for low and medium concentrated magnetite particles on water and one was for high concentrated magnetite particles on various alcohols such as propanol and decanol. The first procedure was for the alcohol based sample, the procedure consisting of the co-precipitation of Fe (II) and Fe (III) ions at 80ºC. Oleic acid was then used as primary sterical stabilisation, also at 80ºC. The excess oleic acid was decanted and was then dispersed in a hydrocarbon. Again, decantation was conducted in order to remove the excess oleic acid. This was then followed by secondary stabilisation with DBS (dodecylbenzensulphonic acid). The particles were then finally dispersed into the alcohol carrier. This double layer sterical stabilisation method was applied as chemically pure Oleic acid was used as the primary surfactant (chemisorbed) and the technical grade DBS as the secondary (physically absorbed) surfactant. This procedure was shown to be very efficient in obtaining a very concentrated magnetic fluid with the saturation magnetisation up to and between 0.6-0.65 A/m.

The second procedure was water based. The magnetite was produced again by a co-precipitation method of Fe (II) and Fe (III) which was added to the NaOH at 80ºC. This was then washed and purified with a double layer sterical stabilisation with DBS again at 80ºC. The particles were then dispersed in water and sonicated. The maximum magnetisation for the water based Ferrofluid was approximately 400G. With increasing volume fraction of particles the stability decreases. The presence of agglomerates can be seen by the greater initial susceptibility compared to that of the propanol sample.

The synthesis of Mn-Zn ferrite ferrofluid has been presented by Auzans et al (1999), the characterisation of these ferrites was also presented. There were two types of ferrofluids that were synthesised, one being a surfactant hydrocarbon-based ferrofluid and, the second being an aqueous cationic ferrofluid.

The synthesis of the ferrite was conducted via the chemical co precipitation method of aqueous solutions of $MnCl_2$, $ZnCl_2$ and $FeCl_3$ in an alkaline medium. Three different alkaline mediums that were also used: sodium hydroxide, methylamine and ammonia. It was seen that for the sodium hydroxide and methylamine that if the zinc concentration was increased in the ferrite then smaller particles were eventually formed. It was also

seen that the biggest size of the ferrites were synthesised with sodium hydroxide, whereas ammonia produced the smallest.

Zn substitution is limited to $0<x<0.5$ and $0<x<0.2$ for methylamine and ammonia formation of ferrite particles. It was also seen that with an increase of Zn, the magnetisation decreased.

2.5: Measuring Velocity:

Love et al (2004) proposed a Magnetocaloric pump for micro-fluid applications. Ferrofluids with Magnetite based in oil were utilised with a Curie temperature of approximately 565ºC and MnZn Ferrite based in water and oil with a Curie temperature of approximately 150ºC.

The experiment that was conducted by Love et al was carried out in such a way that the only variable was the ferrofluid itself. The heat input, the magnetic field and the temperature gradient within the pump was kept at a constant.

A 2mm diameter glass tube was used in this experiment and the results that were obtained showed a maximum velocity of 2.1 mm/s that was obtained for a temperature gradient of 13ºC and of a maximum temperature of 59ºC for a water based ferrofluid.

The velocity of the fluid (V) was measured using a digital video camera and the displacement and the time were recorded. Velocities were also calculated by using Finite-Elemental Analysis (VFEA). The two calculations were then compared. The calculations showed that the ferrofluid that is water based have a velocity of more than an order of magnitude higher than that of a ferrofluid that is oil based. This shows that the MnZn ferrite ferrofluid is a good candidate for Magneto-caloric energy conversion.

2.6: Surfactant:

There has been some difficulty that has been associated with preparing the magnetic fluid. This is because the particles have a large surface to volume ratio and therefore they tend to aggregate. This occurs because the particles want to reduce their surface energy. Magnetic metal oxides have very high surface energy (>100 dyn/cm) making the synthesis of these particles challenging (Shen et al 1998.) Dipole-dipole attraction also takes part in between the magnetic particles increasing the chance of agglomeration. One of the main obstacles in synthesising stable ferrofluid is trying to overcome this agglomeration. This can be done either by physical grinding or a chemical reaction that is

used in their production. This chemical reaction involves the surfactant that has been used within this research.

Several studies have taken place where complex microstructures have been used as reactors in order to obtain ultra-fine magnetic iron oxide particles. It has been mentioned that constrained cavities that are within micro-emulsions or unilamellar vesicles provide much more effective control over the crystal growth, and they prevent particle agglomeration due to free precipitation methods.

However, it does need to be remembered that there is very little control on the average size and the size distribution of the particles.

The suspensions within the magnetic fluid can be stabilised by coating the particle surfaces with organic surfactants. When two particles approach each other, the coated particles with surfactant interpenetrate and the particles are then subjected to steric repulsions due to an osmotic pressure.

In the early 1980s the bilayer stabilisation was proposed by Shimoiizaka et al 1980. Oleic acid was used first, and the precipitated particles were then re-dispersed in an aqueous solution of sodium dodecyl benzenesulfonate, poly(oxyethylene)nonylphenyl ethers, or di(2-ethylexyl)adipate. Shimoiizaka (1980) had hypothesised that the second surfactant coated the primary surfactant coated particles to form a structured surfactant bilayer. Khalafalla and Reimers (1980) and Wooding et al (1988) had followed the work and produced stable aqueous magnetic fluids using various saturated and unsaturated fatty acids as the primary and secondary surfactants. There has been much research that is focused on the synthesis of magnetic particles that are stabilised by the surfactant bilayers, but very little research has taken place regarding the stabilisation mechanism that underlies such systems in terms of the interfacial interactions that might exist.

The quantitative experimental characterisation of the surfactant bilayer is still rare, and the results that are obtained are not consistent with each other.

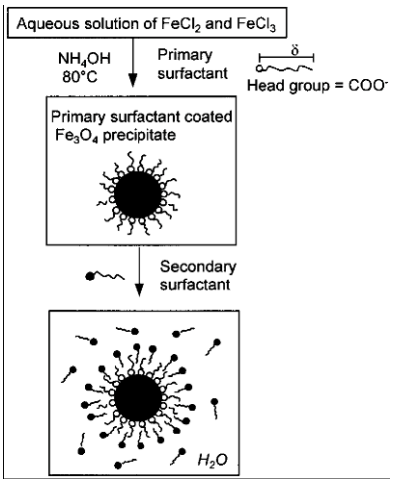

Figure 8: A representation of the synthesis of surfactant bilayer that stabilizes magnetic fluids (Hatton et al , 1999)

The surfactant bilayer can be divided into three zones: The innermost zone is composed of the primary surfactant. The middle region is a combination of the inner and outer surfactant. The outermost zone is composed of the secondary surfactant.

There have also been many other forms of surfactant that has been addressed in the literature. Hatton et al (1999), for the synthesis of water based magnetic fluid of the magnetic nanoparticles, had used two different types of surfactant. One was Decanoic acid and the other was n-alkanoic acid, used as the primary and the secondary respectively. This can be seen in Figure 8.

Now consider the role of surfactant and inter-particle interactions of Mn-Zn ferrite nanoparticles. Two different surfactants were researched by Srikanth et al (2005): bis-(2-ethylhexl) sodium sulfosuccinate, which is referred to as AOT; and a mix of nonylphenol poly(oxyethylene) and nonylphenl poly(oxyethilene), referred to as NP. The stoichiometry of the particles was determined by ICP (Inductively Coupled Plasma) analysis and the results showed a slight loss of Zn for the AOT sample $Mn_{0.68}Zn_{0.25}Fe_{2.07}O_4$ while the NP sample for stoichiometry analysis was $Mn_{0.68}Zn_{0.38}Fe_{2.07}O_4$. TEM studies were also conducted for both samples and the average particle size was shown to be approximately 20 nm for both, whilst the Scherrer analysis of the XRD shown the crystalline size AOT being much larger of 14.6 nm and NP being 10.8 nm.

In particular two surfactants were considered to be the strongest candidates for this research, oleic acid and tetramethylammonium hydroxide. Surfactants can generate either a steric or electrostatic repulsions between the magnetic particles. Oleic acid is

considered to be better suited for oil based ferrofluids as a surfactant that produces steric repulsions. A surfactant coating is created over a magnetite particle with Oleic Acid as it is a long chain hydrocarbon with a polar head that is attracted to the surface of the particle. The prevention of magnetite particles coming close together is due to the tails of the long chain that acts as a repellent cushion. (see figure 9)

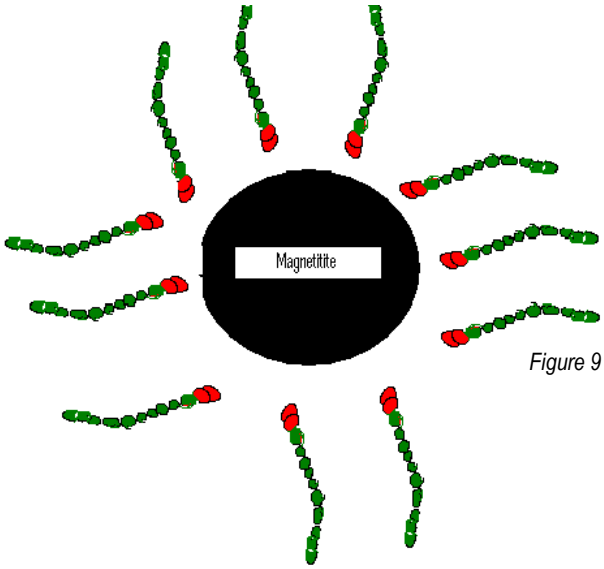

Figure 9 Showing Oleic acid being attracted to a Magnetite particle.

Tetramethylammonium Hydroxide can be used as a surfactant for aqueous mediums as it is ionic and produces electrostatic repulsions. A negative layer over the particle is first formed as the hydroxide ions are attracted to the surface of each magnetite particle. The cations of the tetramethyl ammonium are then attracted to the negatively charged layer, forming a positive layer. When the magnetite particles approach each other they tend to repel due to their positively charged layers. (see figure 10).

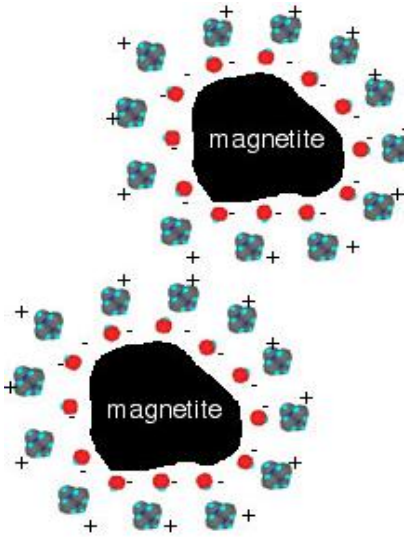

Figure 10: Showing Tetramethylammonium Hydroxide being attracted to Magnetite.

2.7: Characterisation Methods:

2.7.1: SEM (Scanning Electron Microscope)

In the SEM, the electron source is usually a small tungsten tip. Electrons are accelerated to an energy which is usually between 1 ke V to 30 ke V. In order for it to form the smallest probe, electron optics are used to magnify the size of the electron beam. This is achieved by using a series of condenser lenses and a final objective lens, to create a probe forming lens. The condenser lens demagnifies the electron beam and the objective lens provides the final demagnification. It focuses the beam onto the surface; and when it hits the specimen the diameter could be as small as 2-10μm.

The image resolution at a high magnification is approximately equal to the width of the probe. There are a few limitations such as the objective lens. This is due to the lens working at a large convergence angle, the brightness of the electron source, and the interaction volume especially when the samples are not thin.

Blurring of the image may occur due to spherical aberration, due to lens imperfections; which limits the beam focussing. Rays that travel far from the optical axis due to spherical aberration are focused more strongly than those rays that are close to the axis. An objective lens aperture reduces this effect as it is used to limit the angle of the outer rays through the lens. As electrons with slightly different wavelengths are focused more or less strongly, the chromatic aberration may also blur the image. These effects may be limited by using electron beams with narrower energy distribution. Now, the energy distribution of the beam in a microscope is usually less than 2eV for a thermal source and less than 1eV for field emission sources.

Another parameter that limits the resolution is the conservation of brightness throughout the microstructure column. This means that the current is going to decrease at the same time as the electron probe.

There are a number of approaches that may help improve resolution in SEM, increasing the source brightness, decreasing the lens aberration, developing an electro-optical correcting, or by improving lens design by which optical aberrations may be reduced. See Figure 11.

Figure 11a: Picture of SEM taken at the University of Wyoming

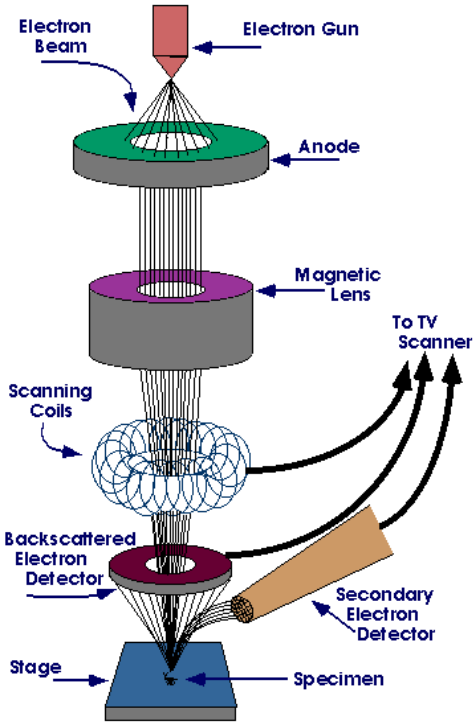

Figure 11b: Picture above taken at the University of Wyoming showing the Scanning Electron Microscope (SEM) and below the components of the SEM instrument

2.7.2: TEM (Transmission Electron Microscope)

The development of the TEM took place in the 1930's, after the discovery of what affect the wavelength has on the theoretical resolution. A TEM probes the internal structure of solids and shows images of the micro-structural or ultra-structural detail that cannot be seen by the human eye. Solid-state materials can be investigated by TEM, as it enables the observation and characterisation of the internal microstructure of a material. The TEM also offers very high resolution that is not offered by any other experimental technique.

This is due to and is possible due to the short wavelength of the electrons. It does not only have information about the chemical composition (analytical electron microscopy) but also about the structural information (e.g. crystalline and crystal structure). This is enough to fully characterise a solid-state sample on a nanometre scale.

TEM is an electron microscope that is analogous to light microscopes; except that the specimen is illuminated by an electron beam. As air molecules scatter electrons the TEM needs to be in a vacuum.

TEM is made up of different components, including an electron emission gun that generates the electron beam. The electron beam gun tends to be thermionic, and allows the acceleration of electrons through a selected potential difference within a range of 40 to 200 kV. The potential difference usually depends on the information that is needed and the nature of the specimen. For example, higher electron energy is needed for samples that are relatively thick or require a very high resolution. The sample should relatively thin, as an electron must have enough energy to pass through the sample; also needs a high accelerating voltage.

A TEM also has a series of lenses that are able to work both magnetically or electro-statically. A specimen stage in a TEM is designed in such a way as to include airlocks. This enables the sample to be inserted in the specimen holder and thus into the vacuum with a minimal increase of pressure throughout the microscope.

Apertures are small annular metallic plates that exclude electrons that are further away than a fixed distance from the optical axis. If there is an absence of specimen, and the aperture is centred on the optical axis, a bright background is seen. This is known as bright field imaging. Parts of the specimen that have a higher density, or which are thicker, will scatter more strongly and would be darker in the image. The diameter of the aperture is determined by the focal length and thus magnification of the objective lens. The diameters that are usually available are 20, 50 and 100 μm.

The image contrast in TEM is due to electron scattering. In the bright field electrons that are scattered to a large angle by the sample do not contribute to the image. Diffraction contrast is given in ordered or crystalline materials, where it is strongly dependent on crystal orientation. In amorphous materials, the image brightness depends on the local mass thickness. The darker regions in bright field imaging are due to regions of higher scattering. The contrast is greater at small objective aperture diameters and at a low

accelerating voltage. Phase contrast may be able to produce an image that is contributed by the scattered electrons. This is very important in high resolution work; where the sample is imaged out of focus to improve on the contrast.

Dark field images normally have a much higher contrast than bright field imaging, but they are much weaker in intensity. In amorphous samples the dark field images are particularly low in intensity, due to the electrons being scattered in all directions and by the objective aperture being able to collect only a few of them. By tilting the incident beam scattered electrons may be collected for the dark field imaging. This is conducted by the electron diffraction pattern of a crystalline specimen that is displayed on a fluorescent screen, and where the required scattered beam is seen, the incident beam is tilted. The tilt is chosen in order to bring the incident beam to the original position of the scattered beam, and the opposite scattered beam to the centre, to pass through the aperture. Dark field imaging gives information about the crystalline structure that cannot be seen in the bright field imaging. In the dark field crystalline dimensions can be measured and their orientation determined. Dark field imaging of polymers may be unstable and may require long exposures to record.

The TEM microscope can also gather chemical information about solid state samples; this is conducted by three different analytical techniques: energy dispersive X-ray analysis (EDX); electron energy-loss spectroscopy (EELS); and high-angle annular dark field imaging (HAADF). See Figure 12.

Figure 12: An image representing a JEM 2100F TEM microscope found at JEOL.

2.7.3: ESEM (Environmental SEM)

The Environmental SEM was produced due to the need for high vacuum in electron microscopes, which gives restrictions to the way samples are prepared and imaged. In the early years of electron microscopy studies were conducted to find ways to image samples in a more natural state. In the late 1950s experiments were conducted on aperture limited, differentially pumped TEMs, i.e. environmental chambers were created. Research that was conducted by Danilatos and Robinson (1979) found that the SEM was capable of maintaining a relatively high pressure; and this led to samples not needing to be dry and coated. The introduction of the environmental SEM was not well received. It was assumed that the resolution would be deteriorated by the gaseous environment, by the assumption of the broadening of the electron beam, and by the exclusion of the secondary electron detection mode of imaging as the ETD induces arcing in the presence of gas. In order to prove that ESEM was a valid microscopy technique the two issues had to be resolved i.e. reduced resolution, and the exclusion of the secondary electron detection. This was resolved by:

1. At elevated pressure the electron probe diameter remains small.

2. Invention of the GDD (gaseous detection device), where the signal-gas interaction that produces gaseous ionisation is used for imaging. The GDD came to be known as GSED (gaseous secondary electron detector) showing that it was possible to detect secondary electrons in the ESEM.

Over the next two decades the ESEM was further developed where it became a benefit to the rest of the scientific world and thus becoming a stable environment.

In order for wet, oily and non-conductive samples to be examined without any preparation an Electron Scanning Electron Microscope can be used. The environment of the sample chamber is varied through a range of temperature, pressure and gas composition. An ESEM microscope is usually operated at a range between 1 to 10 torr, whereby it overcomes the problems of examining samples that are associated with vapours or volatile components. The samples that are characterised in our research are conductive samples due to their magnetism. Even though the ESEM is a good tool to use for characterisation, in order to see the ferrofluid in its natural form, due to its conductivity it may not be the most suitable tool.

In the case of liquids, classical wet mode in the ESEM only allows the characterisation of the surface of the sample, which is usually very smooth; therefore very little information from the sample can be obtained. This is why the wet-STEM described below maybe a better method to characterise aqueous samples. See Figure 13.

Figure 13: An image representing an ESEM machine, from Queen Mary University Lonfon.

2.7.4: Wet STEM

A few years ago in an experimental collaboration, Bultreys and Thollet became the pioneers of wet STEM microscopy (A.Bogner et al, 2005). This occurred in GEMPMM lab based in Lyon. A TEM grid was placed upon a peltier stage of an FEI XL 30 FEG ESEM; with the dipolar detector that is usually used for backscattered electron detection relocated below the grid. This configuration is also used in the high vacuum STEM detector, but was adapted for the use on the cooling stage [6] (see figure 14).

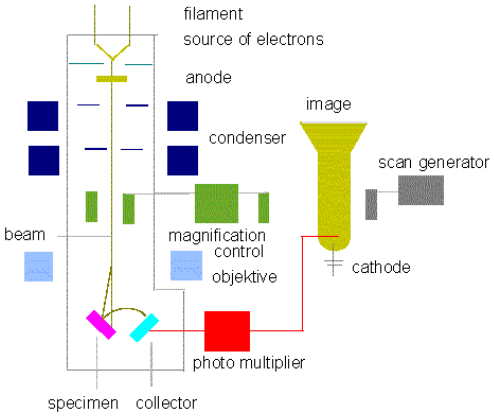

Figure 14: Schematic look of the Wet STEM.

In a classical ESEM microscope, due to imaging conditions, only the top surface of a sample may be imaged. This is due to lattices that are in colloidal state or microorganisms that are not only wet but are also completely submerged in a liquid phase. There also may be drifting of objects. The main difficulty observation in an ESEM microscope faces is the fast damage to the sample under an incident electron beam. Wet STEM was developed in an ESEM and was developed for the transmission in imaging of suspensions. These are objects ranging from nanometres (nm) to micrometres (μm) in size, which are stabilised in a liquid phase, lattices (latex= colloidal suspension of a polymer particle in an aqueous solution) or emulsions (droplets of liquid dispensed in another liquid phase) [10].

Due, to the limitations that are faced in an ESEM (as mentioned above) a wet STEM would be an ideal microscope to image the magnetic Ferrofluid in this study.

This is because a wet STEM allows transmission observations of wet samples in an ESEM. Under annular dark field imaging conditions all sorts of objects are able to be observed. Slow scanning high definition of particles can be performed imaging diameters that are down to a few nanometres.

In operation, a round cylindrical SEM mount is positioned on a peltier stage, where on the head of a TEM sample holder a TEM copper grid is placed upon it and fixed on the aforementioned mount. Before, the copper grid is placed upon the head of the TEM sample holder it is dip coated, the copper grid being submerged into the sample for thirty seconds.

Through the sample an incident electron beam is passed, and the signal is thus collected by the detector. This detector is located below the sample and is usually used for the collection of backscattered electrons. A carbon coated copper grid is used; as the copper squares are used as a retention basin. The typical diameter of the holes range from less than 1μm to 20μm, which allows the overhanging of the liquid films to be maintained on very small areas.

Both gaseous SE detectors (GSED) and gaseous back scattered detectors (GAD), which are classical ESEM detectors, are available. This enables the control of the sample surface in both the SE mode and BSE mode. These detectors also help to see if the objects are submerged in water, by controlling the presence of the liquid, the thickness is

also controlled and it enables the detection of the objects helping to see if the objects are submerged in the water or not.

In order to prevent evaporation and condensation on the sample an optimised pump down sequence is used. Many parameters are also carefully controlled during the sequence, including sample temperature, water source bottle temperature, number of pumping and flooding cycles, initial relative humidity rate in the microscope chamber, and the upper and lower pressures for the purge.

In order for both transmitted and scattered electrons to pass through the water layer, and to be collected in order for the formation of a STEM image, the water layer needs to be kept thin enough. This can be done by adjusting the pressure and temperature, which is then followed by a small amount of water being evaporated from the droplet. Evaporation is an endothermic reaction; and a constant check can be kept on the changes by checking the differences between the setting temperature and the measured temperature. The thickness of the sample is determined by the quantity of water that is evaporated from the initial droplet. This initial droplet volume and initial solid content are known due to the solid content of the sample being controlled. An equilibrium water pressure using the (P, T) water diagram is used to keep the thickness of the water layer constant. Samples can be kept above their saturated vapour pressure during an experiment by the temperature of the sample being controlled through the peltier stage, and at a controlled pressure using the water vapour as the imaging gas.

In the SEM mode the detection strategy is conducted by the electrons being collected directly through the sample via a solid state detector (two semi-annular detectors A and B). In the STEM mode both bright field and dark field images can be produced by the collection of scattered or transmitted electrons via the incident electron beam arriving on the limits of the diodes A and B. In this case there is not a choice for the imaging mode, as only a small area of the sample is above the border of the diodes A and B. There is also another possibility: If the dipolar detector is placed on the optical axis, annular dark field imaging conditions can be obtained. The direct transmitted electron beam is not collected and only scattered beams are detected on a ring that is made up of both diodes A and B. This method allows the most important part of the scattered electrons to be used to form an image, and higher contrasted images can be obtained as a result.

2.7.5: EDX (Electro Dispersive X-ray)

Electro Dispersive X-ray spectroscopy is an analytical tool for the chemical characterisation and elemental analysis of a sample. The sample is characterised via the interactions of the electrons with matter and analysing the X-rays that are emitted by the matter when it is simulated with a high energy beam of charged particles such as electrons and protons. The main reason for the characterisation capabilities are due to each element having its own unique atomic structure; this being the reason that the X-rays that are emitted from the atom can be uniquely identified.

The X-ray is emitted from the sample when a high energy beam of charged particles such as electrons or protons are focused upon the sample. This is because when the atom within the sample is at rest the electrons in the electron shells are unexcited. This is known as the ground state, where the electrons are bound to the nucleus. The incident beam hits the atom and excites an electron that is within the inner shell, therefore ejecting it and thus creating an electron hole. An electron from the outer shell then fills the hole, the difference between the higher energy shell and the lower energy shell is released as an X-ray. The energy-dispersive spectrometer measures the number and the energy of the X-rays that are emitted from the specimen. The elemental composition of the specimen is measured and characterised, as the energy of the X-rays is the difference between the two shells and is representative of the atomic structure of the elements from which the electron is emitted.

The four main components of the EDX are the beam source, the X-ray detector, the analyser and the pulse processor. Even though free standing EDX systems can be found the majority are found within the SEM. The X-ray energy is converted via the detector into voltage signals, and this information is then sent to a pulse processor. This then measures the signals, which are thus passed onto an analyser for interpretation.

In future work, it is planned for the EDX to be used to analyse the elemental composition of both the Ferro- Magnetic particles and also of the impurities within the sample from two different areas of the samples. This is in order to see how the particles are spread within the sample and to determine the ratio between the unwanted impurities and the actual magnetite. This could help with future improvements of the process in terms of identifying the causes of process failures and how to reduce process variability.

2.7.6: XRD (X Ray Diffraction):

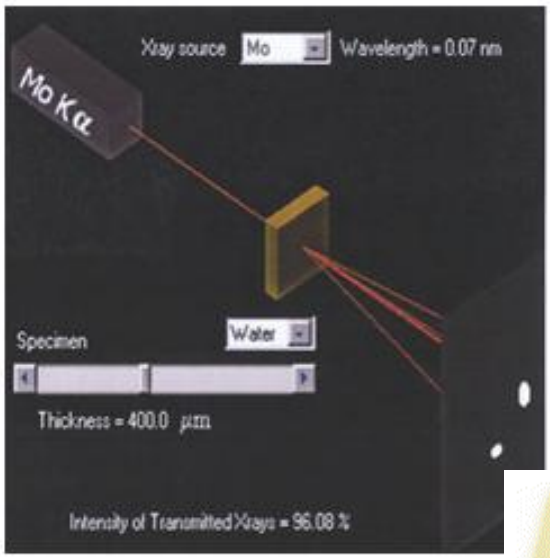

Figure 15: X Ray Diffraction

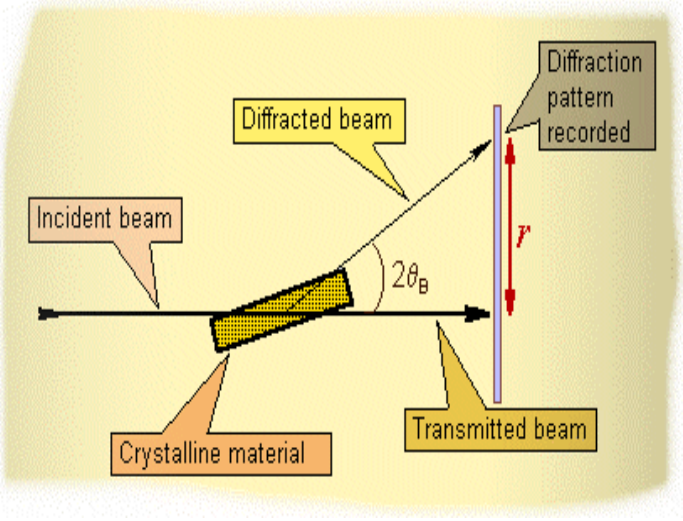

Figure 16: Schematic presentation of how an XRD would work.

X-Ray Diffraction, which is also known as XRD, is when within a crystal the atomic plane causes an incident beam of X-rays to interfere with one another when they are leaving the crystal. When interpreted it gives an idea of the shape of the crystal structure. See figure 15 and 16.

A.W.Hull 1919, wrote a paper titled “A New Method of Chemical Analysis”. It was in this paper that he had mentioned that “every crystalline substance gives a pattern; the same substance always gives the same pattern; and in a mixture of substances each produces its pattern independently of the others” Therefore it can be deemed that the pattern of a pure substance is like a fingerprint of that material.

The size of a small object can have an effect on the behaviour of light waves; this can be seen by an array of sources producing diffraction patterns, whilst two small spaced

objects produce an interface pattern. The patterns are all dependent upon the position and size of the light source. This was thus taken further in 1912 by William Bragg who studied crystal structures using X-rays. He found that when certain geometric requirements were met, the X-rays that were scattered from a crystalline solid are able to cause an interference pattern that in turn produces a diffracted beam. Bragg also established relationships that occurred between different factors. He realised that there is a distance between similar atomic planes in minerals called the interatomic spacing. This is called d-spacing and it is measured in angstroms. The theta angle is the angle of diffraction and is measured in degrees. The measured angle is called 2-theta, as the diffract meter measures an angle that is twice the size of the theta angle. The third factor is the wavelength of the incident X-radiation, which is usually equal to 1.54 angstroms in copper.

These factors are combined in Braggs's Law:

$$n\lambda = 2d\sin\theta$$

Where:

n = an integer - 1, 2, 3..., etc (n=1 for our calculations)

λ(lambda) = wavelength in angstroms (1.54Å for copper)

d (d-spacing) = interatomic spacing in angstroms

θ (theta) = the diffraction angle in degrees

Figure 17: Showing how Bragg law works.Found on: http://www.uhh.hawaii.edu/~kenhon/mineralogy/lab-syllabus/xtal-xray/XRDmethod.html

Working out the structure of a crystal from X-ray patterns is an example of an inverse problem, akin to integration and differentiation in mathematics. In X-ray diffraction there are two methods of using crystals, one being a large crystal and the second being a powder. If a large crystal is being used than the required effects may only be seen for certain positions of the beam and the crystal. The image of the X-ray will be a series of spots on the film. The information from the image is gathered and decoded from the positioning and the brightness information. In using a powder, the positioning may be better and the image from the X-ray would be a set of circles around the beam.

The X-ray diffraction works with the basic idea in that the waves from all parts of the object combine together to form the intensity in any direction. This intensity varies depending on the wave amplitude. The dispersion of waves is bigger for smaller object rather than larger objects.

The diffraction patterns of any crystalline solid can be constructed by using a diffractometer. With this diffraction pattern an unidentified material can be identified, or the atomic-scale structure of an identified material can be characterised. Data has been complied and published by the JCPDS-International Centre for Diffraction Data of existing systematic X-ray diffraction for thousands of mineral species.

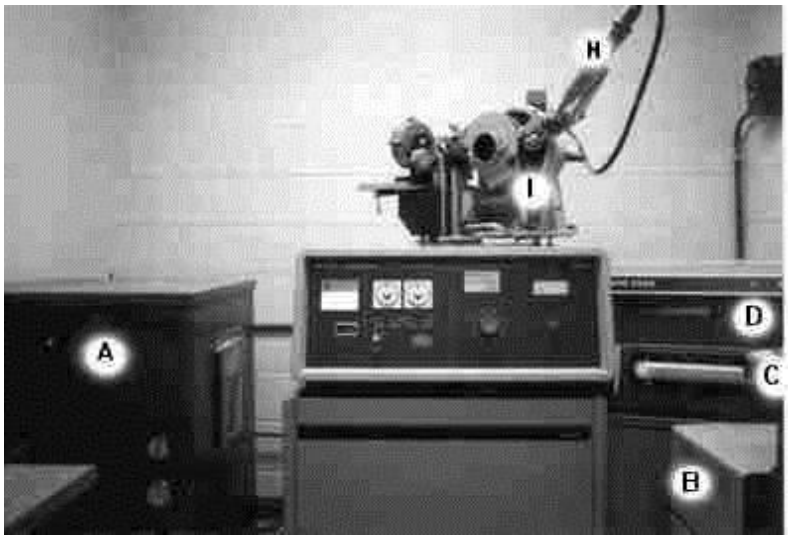

Figure 18: An X-Ray Diffractometer machine, Philipps APD3520.

The diffraction pattern taken with the X-Ray Diffractometer records the X-ray intensity of a 2-theta angle. An example of this is as follows:

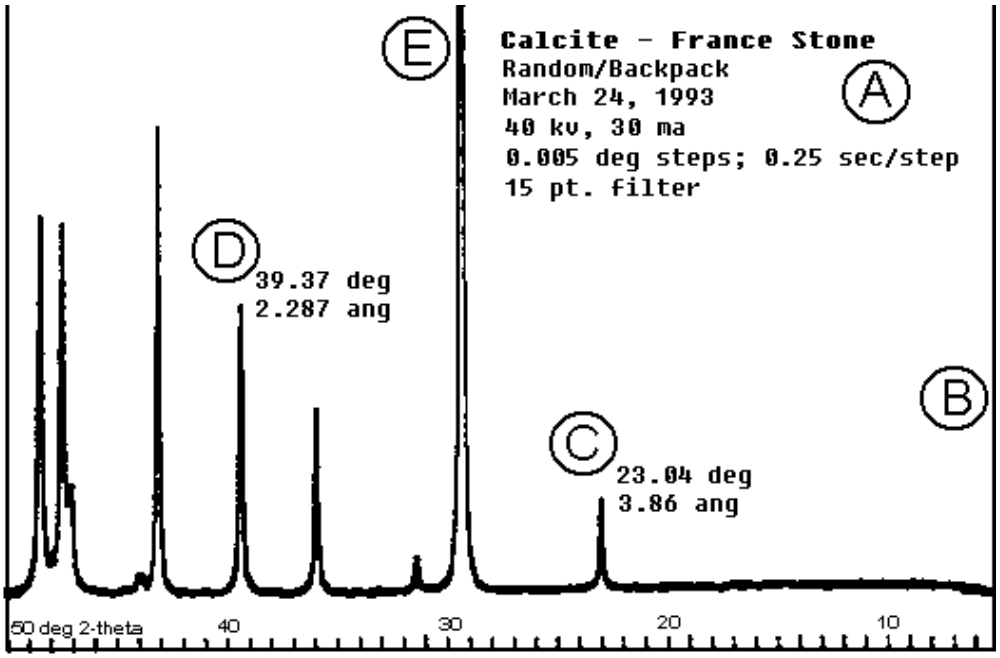

Figure 19: Image of an X-ray Spectrum.
http://www.uhh.hawaii.edu/~kenhon/mineralogy/lab-syllabus/xtal-xray/XRDmethod.html

From this image, the angle of the X-ray can be found as well as the crystallinity of the material and the elemental composition; thus giving an idea of what an unknown material can be with what the crystalline structure is.

3.0: An Application of Ferrofluids: Energy conversion and Regeneration:

(Rosensweig, 1985), showed that energy regeneration from low grade thermal energy loss can occur; and how the properties of ferrofluids can be utilised in a closed system to provide cooling. The fluid is contained within a hermetically sealed system that passes over the source of waste heat. The fluid is below the curie temperature and using an externally applied magnetic field, the fluid is drawn into the heat affected zone; this can be from any waste source. The magnetic properties of the fluid needs to be diminished, this is done by heating the fluid in the region of the curie temperature. A pressure differential in the system is created, which drives the fluid flow. This is because of the change in the magnetisation and the effect of the highly magnetised and cooler fluid behind the heat zone. In order to achieve the greatest pressure differential and a high rate of flow within the system it is necessary to reach a temperature as close to the curie temperature as possible; whilst having the flow within the heat affected zone as cool as possible.
This pressure differential can be created by the following equation:

$$\Delta P = \mu_0 H\ [M(T_{outlet}) - M(T_{inlet})]$$

μ_0 = Permeability of free space

H = Externally applied magnetic field intensity

M(T) = Temperature dependent magnetisation of the particles.

The overall thermal property of the ferrofluids needs to be tailored to each application for an optimised pumping mechanism. The best thermal pumping effect is largely credited to the specific heat capacity and the thermal conductivity of the fluid. Particularly with the carrier fluid used and the particle density, (Popplewell, et al, 1982) has shown a relationship between the fluid formulation and the thermal properties. In, order to maintain the correct flow rate that is needed for conversion, the fluid needs to be able remove as much of the waste heat in each cycle as possible.

One phenomenon that can be considered and that takes place in the magnetic fluid is the magneto-calorific effect (MCE). This is where the material heats up when it is under the influence of a magnetic field. This is because when a magnetic field is applied, the entropy that is associated with the magnetic degree of freedom, i.e. the magnetic entropy (S_m) is changed as the field changes the magnetic order of the material; if this is performed adiabatically, ΔS_m must be compensated by an equal but opposite change of the entropy that is associated with the lattice, resulting in a change of temperature. This temperature change is known as MCE. It is related to the magnetic properties of the materials through the thermodynamic Maxwell reaction. (Kinnary. P et al, 2000), (E.Bruck et al, 2003). The effect occurs due to a disordering of the magnetic domains that occurs under the influence of a decreasing magnetic field, which causes the material to lose some thermal energy.

It has been shown that due to the Magneto-calorific effect it is possible to reach ultra-low temperatures (1K). Recently a focus has been made to find magnetic refrigerants that are able to work at a higher temperature i.e. (T > 20K). The most promising classes of materials are heavy rare earth elements and their compounds, due to their high magnetic moment. This effect is extremely strong in gadolinium formulations. (Zimmerman et al, 2009) noted that the effect can be in the region of 270K to 310 K temperature change per Tesla of applied field strength. The rarity of some of these magnetic materials can cause

a problem and there is a search on ways to achieve the effect whist using minimal resources. How the Magneto-calorific effect will work in the ferrofluid formulation is also uncertain and more work does need to take place in this regard in order for it to be commercially viable. (Tishin et al. 2003).

The ideal energy conversion device should be able to recycle and convert some of the recovered energy back into a viable transferrable power, and provide cooling for a given system. It is hoped that it could be possible for the heat that is absorbed by the fluid to be reused as a heat source for another application, for example heating a building. Another example would be to recycle some of the energy removed from the system by converting the motion of the magnetic fluid into a useful electrical output.

A complete system should contain all the features that have been discussed for a hermetically sealed system tailored for specific heat loss applications. The cool ferrofluid that is below its Curie point would flow past a waste heat source and absorb its heat; this will increase the temperature of the ferrofluid to the Curie point and in turn this will enable the thermal pumping phenomenon. The fluid that is the hottest will continue to flow in the loop and will be removed either by a heat exchange mechanism, to transfer the heat out of the system, or it will be extracted by a radiation method. The cooler fluid that is now back below its curie point will regain its ferromagnetism and this fluid will continue to flow due to the introduction of turbulence to the system either by applying an external magnetic field or using structural features to perturb the flow. The particles are aligned to induce a useable emf in an appropriate circuit (coil) that is proximal to the flow. The cool fluid then returns to the beginning where the cycle starts again where it is reheated by waste thermal energy from the heat source once again.
A factor that does need to be considered is the bulk flow rate through the system. This is because it could have an impact on the heat transfer and the thermal generation. If the flow rate is too high, the system will remain laminar and it will be too difficult to initiate an effective turbulent flow. Also, if the flow is too fast the heat transfer from the waste system may not take place effectively. In order to produce a good pumping effect to satisfy the cooling needs enough heat must be removed from the system in each cycle. It is important to find a way to optimise the turbulence and the flow rate, in order to produce an efficient system.

It is important to confirm experimentally the validity in a controlled environment of each aspect of the system and its many factors, as these could be effects on a scale that is significantly larger than in ferrofluids used in most current commercial applications.

4.0: Ferrofluid Sample Preparation:

During this work, samples of ferrofluids were produced from the reagents ferric chloride hexa-hydrate and ferrous chloride tetra-hydrate for the synthesis of Magnetite (Fe_3O_4). The method that was used was a combination of processes from the work of Arulmurugan et al (2006) and Martinez-Mera et al. (2007). The synthesis of Manganese Zinc Ferrite was also conducted producing $Mn_{0.5}Zn_{0.5}Fe_2O_4$. The Magnetite was made at varying temperatures of 60°C and 80°C with Oleic Acid and Tetramethylammonium Hydroxide, and the carrier fluid being either water or oil, in order to see which would prove the optimum method to produce ferrofluids with little agglomeration, particles size of approximately 10nm to 20nm, and for the surfactant to coat particles uniformly. The Ferrite was synthesised using the two different surfactants that have been mentioned above.

4.1: Synthesis of Magnetite

150 ml of 4M of ammonium hydroxide was produced, 10ml of the solution was retained and the rest was heated in a volumetric flask to a maximum of 80ºC for 15 min. A solution of 25ml of 0.5M was also produced of Ferric chloride hexa-hydrate and ferrous chloride tetra-hydrate which were then mixed together and added to the solution that was left to be stirred with a mechanical stirrer for 50 minutes. A black precipitation was observed, as seen in figure 20.

A 1M solution of Sodium Oleate was produced, to be used as the basis of a surfactant to encapsulate the ferrous nano-particles. The Sodium Oleate was produced via a 3M solution of Sodium hydroxide that was mixed 0.5M of Oleic Acid, this was then added to the solution and left to stir for a further 30 minutes. Evaporation was prevented by the addition of a condenser and a lid to the volumetric flask.

A sample was taken via magnetic separation in order for the magnetite to be characterised. As, seen in figure 21a and 21b.

The samples that were made were produced at three temperatures to see if temperature played at a part during the synthesis of the ferrous nano-particles. Sample one and two were synthesised according to the method that was described above, the main difference being sample one was synthesised at a temperature of 20ºC instead of 80ºC and sample two was synthesised at a temperature of 40ºC.

Figure 20: Picture showing the apparatus set up of producing the Ferrofluid. It was necessary to cover all orfices in order to reduce the formation of rust.

Figure 21a: Showing the result of Magnetite, with a magnet being placed underneath, the magnetic magnetite particles can be seen being drawn towards it.

Figure 22b: Showing the magnetic Magnetite particles being drawn to the magnet underneath.

4.2: Synthesis of Manganese Zinc Ferrite

Mn-Zn ferrite nano particles was prepared by chemical co precipitation by Arulmurugan et al (2006).

It has been mentioned previously that when the Zn concentration is increased in the preparation of $Mn_{1-x}Zn_xFe_2O_4$ to a value of 0.5 then the produced nano particles have a Curie temperature of 160ºC. This is the reason that this stoichiometry has been chosen for our experiment.

The method of preparation was as follows:

A 2M aqueous solution of 50 ml of NaOH solution was prepared and poured into a reaction vessel that was then heated to a temperature of 80ºC.

A 10 ml of aqueous solution of 0.5M $MnCl_2$, $ZnSo_4.7H_20$ and a 10ml of 2M solution of $FeCl_2.4H2O$ was then prepared. All three solutions were mixed together and added to NaOH solution at 80ºC. This was left to stir for a further 30 minutes.

The solution was decanted and then cleaned using distilled water and nitric acid with a concentration of 2Mol/L. After decanting the nano-particles were produced, the cleaning solution was poured into the container and the mixture was agitated for 10 minutes. The mixture was centrifuged at 3500 rpm and the liquid was decanted from the mixture. This was repeated three times. Tetramethylammonium hydroxide was used as the surfactant and a dilute solution was produced of 25% Tetramethylammonium hydroxide to 75% water. The Surfactant was added to the nano-particles in small amounts, 1 ml to achieve maximum concentration. The mixture of surfactant solution and nano-particles was further agitated for 10mins and centrifuged for a further 5 minutes at 1200 rpm. The fluid that remained on top of the precipitated nano-particles was the Ferrofluid.

4.3: Results and Analysis:

The samples were characterised using the SEM and XRD to see what sample could be considered to be the optimum sample and then to compare it to a commercial sample. All the samples were conducted at a high vacuum due to the type of characetrisation methods that were used; they were thinned with Propanol and dried before being placed in the Electron Microscopes. As the samples were dried in order for them to be characterised there is likelihood that some of the properties of the samples may have been lost. A vast difference was also seen between the samples that were synthesized at the beginning of the project to the samples that were produced mid-way. The main difference being less agglomeration and the ability to see the shape of the particles, the particles also in general were much closer to the predicted range of 30 to 50nm. This may be due to the preparation method of the samples, which may have become more accurate and sophisticated compared to the first batch of samples. The dendrite salt formation in later samples had also decreased.

Five samples were produced that had varied conditions such as temperature that ranged between 60°C to 80°C and surfactant. The two that was used were: Oleic Acid and Tetramethylammonium Hydroxide. Oleic Acid was the main surfactant that was used at the beginning of this work; after the production of the first batch of samples and the extent of agglomeration that had taken place it was realized that in water based solution Oleic Acid would produce a “soapy” affect and coat more than one particle. A surfactant had to be used that was suitable for an aqueous medium. Tetramethylammonium Hydroxide was used due to its ionic nature and the electrostatic repulsions that are produced. From, the results it is clear to see that the change of surfactant did improve the level of agglomeration dramatically, and that the change of surfactant had proved to be a success for the aim of this project.

The particle sizes of the samples were determined via the Scanning Electron Microscope. A range of particle sizes were taken around the sample and an average of the sizes were then taken. The average particle size from the samples in this instance proved to be around the range of 30 to 40nm.

The first sample that was characterized was Magnetite with Oleic Acid at 60°C (Figure 23). Agglomeration was found, but the particle size was a lot closer to what the average predicted size would be. In previous synthesis the particle range was approximately 70 to 80nm, and the particle size were in a range between 40 to 50nm. The sample was very thick and could have been placed in the centrifuge in order to thin the sample.

The second sample that was characterized was Magnetite with Oleic Acid at 80°C (Figure 24). A mass of nano-particles and singular particles was seen; again the particle size was in a range between 30 to 50nm. The oleic acid had encapsulated a group of particles rather than just singular ones. This may be because of the amount of Oleic Acid that was added (1m in 10ml of ammonium hydroxide). The amount can be decreased to 0.5ml to see if a difference can be made.

The third sample that was characterized via the SEM was Magnetite with Tetramethylammonium Hydroxide as the surfactant at a temperature of 80°C (Figure 25 and 26).The agglomeration was again present but not to the extent that was previously seen. The particles also appear to be much smaller (i.e. ~10nm) compared to the particles with Oleic Acid as the surfactant. This may be due to the surfactant being diluted with water and not coating the particles properly. The particles seem to be more uniformly spread out compared to the samples with Oleic Acid as a surfactant.

The fourth sample was Magnetite with Tetramethylammonium Hydroxide as the Surfactant and synthesized at 70 °C (figure 27). The particles seem to have been coated more thoroughly in this case and the particle size was at an average of 35nm, again smaller than the particles observed with the Oleic Acid.

The fifth sample was of Ferrite with Tetramethylammonium Hydroxide as the surfactant (figure 28). The particles in this sample looked flatter and more plate-like compared to the magnetite, which appeared to be more spherical. The particles are small in size with an average of 40nm. Instead of forming a “clump” like structure that is seen in magnetite the Ferrite particles group together in a plate like structure. The particles appear clearer compared to the Magnetite structure.

From, previous work a characteristic that had to be considered was the particle size. It had become clear that it was better to synthesize the fluid at a higher temperature compared to a lower one, as it can be seen from this work that particle size at a higher temperature was at an average between 30 to 50nm compared to the micron size that was seen previously. It can also be seen that Tetramethylammonium hydroxide acts as a better surfactant, as the coat on the particles is more thin compared to the Oleic Acid and there is much less agglomeration that is present compared to the Oleic Acid.

Looking at the TEM samples it was seen that less clumps were produced in the commercial sample and the particles in the commercial sample was more uniform compared to the synthesized particles. The sizes of both were at an average of 30nm. It is also interesting to see that the TEM provides a clearer picture of what the particles look like compared to the SEM.

In future work it would be very interesting to see the samples in its natural form rather than the SEM or the TEM as the samples are characterized after being dried and in high vacuum where some of its properties can diminish. The Magnetite in oil also needs to be characterised, the method of preparation of this needs to be looked at, as the samples that were produced were too thick and proved very difficult to dry - therefore not allowing any characterisation to take place.

It would also be interesting to synthesize the Ferrite in a larger volume and to measure the Curie temperature. This is due to the Curie Temperature of Magnetite made from Iron being 585°C and the Ferrite being made from Manganese-Zinc being 180°C, it is therefore easier measuring the temperature up to 180°C rather than 585°.

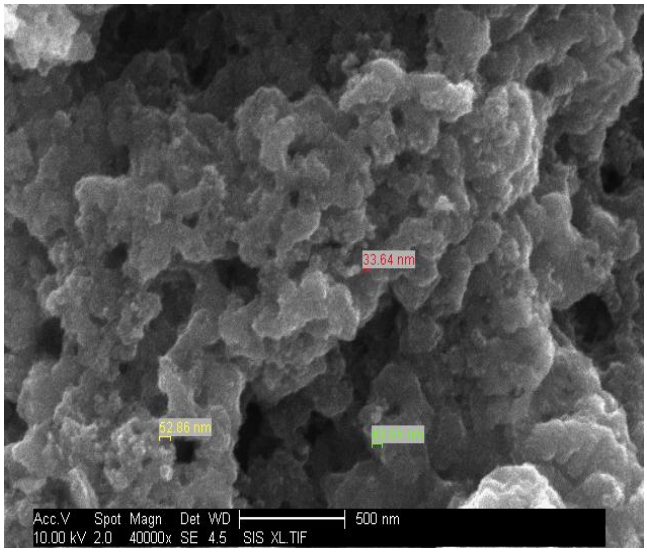

Figure 23: Sample one of Magnetite at 60C in Oleic Acid at approx.124x

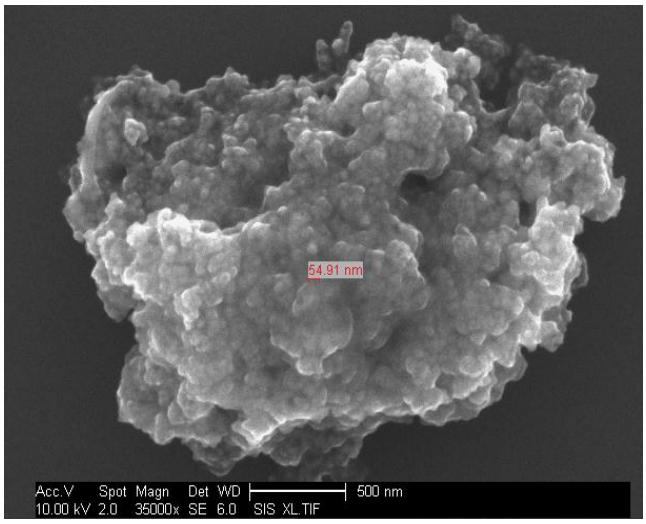

Figure 24: Sample Two of Magnetite at 80C in Oleic Acid at approx. 124x

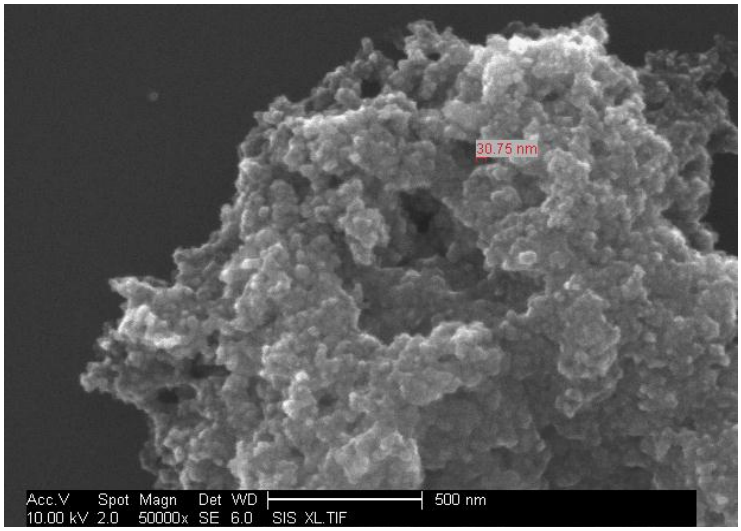

Figure 25: Sample three of Magnetite at 80C with Tetramethylammonium Hydroxide at approx.144x

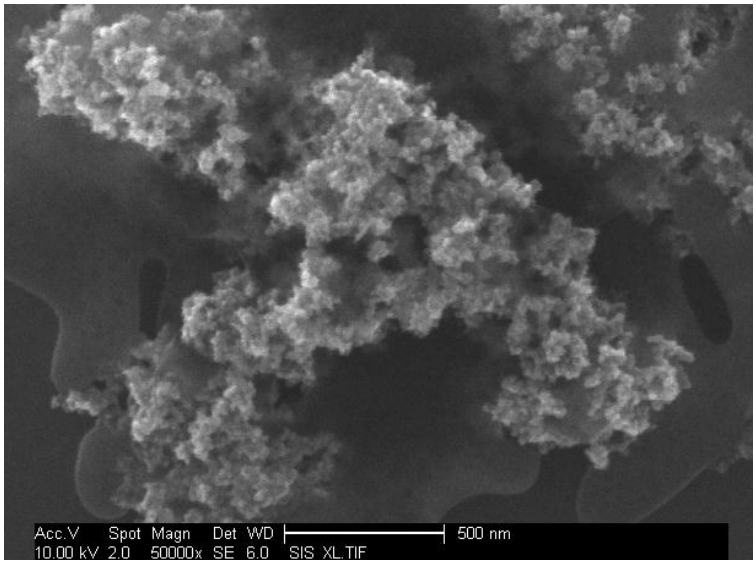

Figure 26: Sample three of Magnetite at 80C with Tetramethylammonium Hydroxide at approx.144x.

-

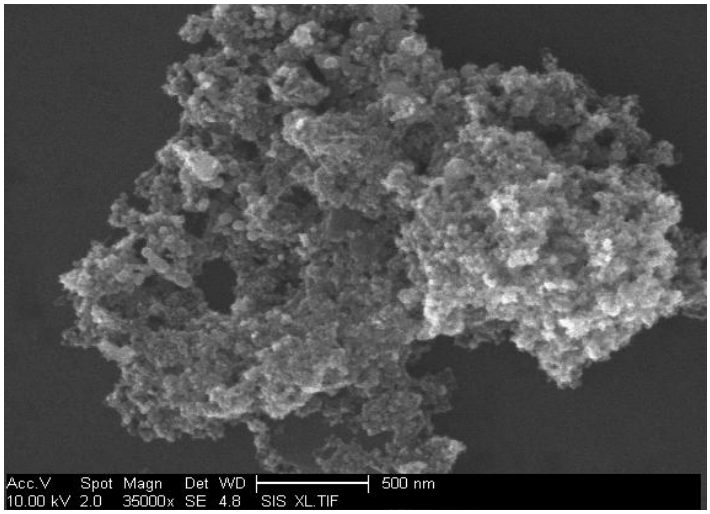

Figure 28: Sample four at a magnification of at approx.138x.

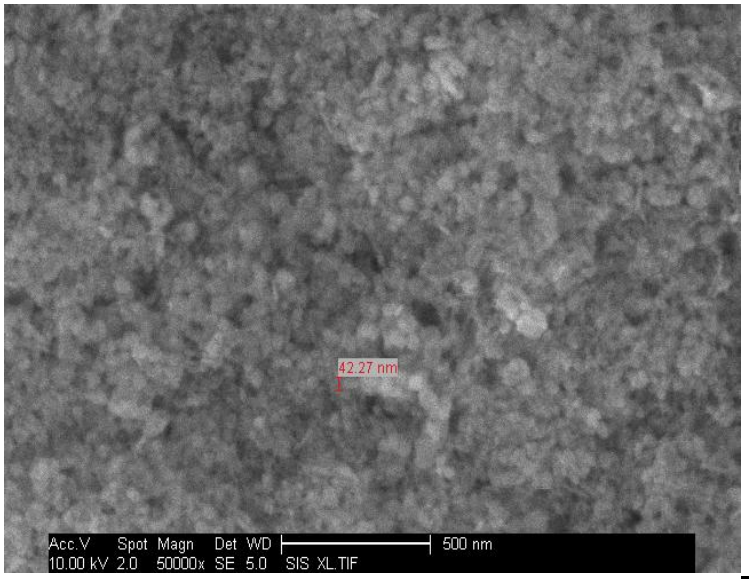

Figure 29: Sample four at a magnification of at approx.144x.

5.0: Ferrofluid Synthesis: An analysis of process variables using Statistical Design of Experiments (SDOE)

5.1 Experimental Design

Statistical tests provide tangible benefits, including the identification of key process variables. This is deduced from a series of statistically designed experiments.

The benefits of implementing the statistical tests could be the elimination of unacceptably high scrap and rework in the technical process. It could also reduce inspection time and any tests that are non-value added operations. It can also eliminate the need of unplanned equipment or process down time. This would also reduce the manufacturing cycle time. (K. Bhote, 1988).

The statistical methods used here come under the heading of Design of Experiments (D.O.E). The objective of D.O.E. is to discover the key variable in product and process design, to drastically reduce the variations they cause, and to open up the tolerances on the lesser variables so as to reduce costs. (K. Bhote, 1988).

The technique within D.O.E that was relevant for this work was the Fractional Factorial Design as there was four variables. The motivation for fractional factorials is usually the large number of factors that tend to make the number of process runs for designs grow quickly. The emphasis of these statistical tests becomes the factor screening, where the factors with the large effects are found efficiently. There are usually many variables that are run as un-replicated factorials, and usually with a centre points. The subsets in the Fractional factorial design are chosen so the scarcity-of-effects principle (where there may be may factors, but only a few are important or the system is dominated by main effects, low-order interactions) in order to expose the information about the most important features of the problem studied. This is done whilst using a small amount of the effort of a full factorial design when considering the experimental runs and resources.

Notations for Fractional design are expressed as: l^{k-p}.

l is the number of levels of each of the factors are investigated.

k is the number of factors investigated.

p describes the size of the fraction of the full factorial that is used.

Previously *p* was considered to be the number of generators where the effects or interactions were not able to be estimated independently of each other.

The levels of a factor for this design are normally coded as +1 for the higher level, and -1 for the lower level. If the factor is three-level, the intermediate value would be coded as 0.

An alias structure is chosen for a full factorial experiment in order to generate a useful fractional factorial experiment. This alias structure is what determines what effects are

confounded with one and another. For example, by using a full three factor factorial experiment where three factors are involved (for example: A,B and C) for the five factor 2^{5-2} and these factors are then confounded by two remaining factors D and E with the interactions are thus generated by D=A*B and E=A*C, which is known as generators of the design. The effect that is being investigated and estimated in this case would be the combination of the main effect of D and the two-factor interaction involving A and B.

Defining the relation is an important characteristic of a fractional design. A relation gives the set of interaction columns that is equal in the design matrix to a column of plus signs that are denoted by *I.* The resolution enables the main effects to be separated and have low order interactions from one another. The resolution of the design is formally the minimum word length in the defining relation that excludes 1. III, IV and V are the most important fractional designs. Resolutions that are above V are wasteful as they can estimate very high order interactions that very rarely occur. Resolutions that are below III are also not useful. As can be seen by below:

Table 1 showing the resolutions and factors, taken from G.Box, et al (2005)

Resolution	Ability	Example
II	Not useful: main effects are confounded with other main effects	2^{2-1} with defining relation I = AB
III	Estimate main effects, but these may be confounded with two-factor interactions	2^{3-1} with defining relation I = ABC
IV	Estimate main effects uncompounded by two-factor interactions Estimate two-factor interaction effects, but these may be confounded with other two-factor interactions	2^{4-1} with defining relation I = ABCD
V	Estimate main effects unconfounded by three-factor (or less) interactions Estimate two-factor interaction effects unconfounded by two-factor interactions Estimate three-factor interaction effects, but these may be confounded with other two-factor interactions	2^{5-1} with defining relation I = ABCDE
VI	Estimate main effects unconfounded by four-factor (or less) interactions Estimate two-factor interaction effects unconfounded by three-factor (or less) interactions Estimate three-factor interaction effects, but these may be confounded with other three-factor interactions	2^{6-1} with defining relation I = ABCDEF

In this work the resolution that was used was IV, with four factors, 2 levels and 8 runs with the Alias Structure being: I+ABCD. The limits that were used were the main four factors that were considered in this work that may affect the properties of the ferrofluids. The four factors were the surfactant, the temperature, the time and the concentration. This is due, to the different number of extents for the process of producing a ferrofluid that produces less agglomeration, particle sizes that are more uniform and a fluid that is re producible a statistical test was conducted concentrating on four different parameters. The parameters were temperature at two extents 60°C and 80°C, time at 15 minutes and 30 minutes, two different surfactants Oleic Acid and Tetramethylammonium Hydroxide and Concentration.

Factor	Name	Low (-1)	High (+1)
A	Surfactant	Tetramethylammonium Hydroxide	Oleic Acid
B	Temperature	60°C	80°C
C	Time	15 Min	30 Min
D	Concentration	Previous Concentration 1	New Concentration 2

From the test eight different methods were by formed by randomly applying the different parameters. The tests that were produced were as follows:

Table 3: showing the statistical tests and the different parameters.

Tests	Method
1	-1,1,1,-1
2	1,-1,-1,1
3	-1,-1,1,1
4	1,-1,1,-1
5	1.1, 11
6	-1,-1,-1,-1
7	-1,1,-1,1
8	1,1,-1,-1

From the above table the usual method of the chemical co precipitation method that was adapted by the method that was used by R. Arulmurugan was used in conjunction with the parameters in order to find the method that produced the best ferrofluid.

6.0 Results: Characterisation of nanoparticles

6.1: Characterisation of Particle Size:

A nanoparticle based within a ferrofluid that is produced by a chemical synthesis displays a particle size distribution that is broad. This may be due to the thickness of the coatings, the variations in the core size or because of the different stages of agglomeration. The magnetic properties of a nano scale ferrofluid are determined by the particle size, particle shape, particle size distribution and the particle interaction. To obtain customisation of the ferrofluid for a specific application it is important to understand these parameters thoroughly. Therefore, in order for us to understand these properties better it is vital for us to understand what methods would help characterise and give a better understanding on how they function.

The magnetic properties of the nanoparticles usually depend on the volume of the fluid, which is a function of the particle diameter and the shape. Two mechanisms can be distinguished for the relaxation of the magnetic nanoparticles, one being the Brownian relaxation where within the carrier liquid there is entire diffusional rotation of the entire particle. Alternatively there is, Néel relaxation, where within the particle is the rotation of the cores magnetic moment. This is shown by the amount of magnetic material contained and is proportional to the magnetic moment of a single domain; i.e. the particle volume increases with the magnetic moment thereby with the third power of its diameter. The rotational diffusion time τB is attributed to the Brownian relaxation of a spherical particle that is given by (Langmuir et al)

$$\tau_B = \frac{3\eta V_h}{kT}$$

Where *k* is the Boltzmann's constant, η is the viscosity of the surrounding liquid, T is the temperature and V_h is the effective volume of the whole particle. In contrast to this, the Néel relaxation time τ_N of the magnetic moment within the particle for particles with uniaxial anisotropy is given by (Langmuir et al):

$$\tau_N = \tau_0 e^{KV_c/KT}$$

Where V_C is the volume of the magnetic core and where τ_0 is a constant that is usually assumed to be in the range of 10^{-9}s. K is the effective anisotropy constant that usually

regarding the shape, crystallography or the surface anisotropy. In this case the effective anisotropy usually results from their shape anisotropy. (Langumir et al, 1998)

A liquid that contains magnetic nanoparticles would align to the direction of the magnetic field when an external magnetic field is applied therefore creating an ensemble of a net magnetic moment. When this applied magnetic field is switched off, the net magnetisation would disappear due to the nanoparticles reorientation occurring with an effective relaxation time τ_{eff}. This is given by:

$$\tau_{eff} = \frac{\tau_B \tau_N}{\tau_B + \tau_N}$$

Thereby, showing the faster mechanism dominates.

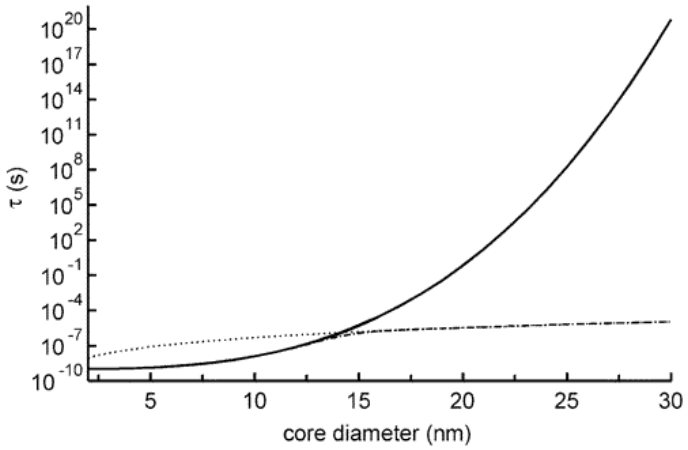

Figure 30: Dotted line representing Brownian and straight line representing Néel; showing the comparison of both and also the effective relaxation time (dashed line) on the particle diameter of spherical magnetic nanoparticles. Assuming K= 20kJ/m^3, T= 300K, η= 1 mPa s.

The above graph illustrates the mechanism mentioned. The different relaxation times are plotted for the magnetite nanoparticles that are dispersed in water, assuming the anisotropy for the magnetite being uniaxial. It is also assumed that both the hydrodynamic diameter and the core diameter are both the same. Therefore the effective anisotropy of the magnetite particles was determined to be in the range of 1x10^4 and 4x10^4 Jm^{-3} (Buescher et al). It can be seen that the relaxation time of the magnetic vector is dependent on the particle core diameter. Below core diameters of an approximate 13nm, Néel relaxation tends to be faster and for the particles that are larger in size Brownian relaxation is what dominates. Therefore concluding that if an application of a Ferrofluid is needed where the relaxation behaviour of an immobilised particles is important, as the Néel relaxation time increases exponentially with the particle volume, even a slight

change in the particle size may have a dramatic effect. An example of these using magnetic nanoparticles for storage of magnetic recordings where the particles are fixed and only Néel mechanism is possible. Recording media that are prepared from particles in the size range of 21nm will lose the information in less than 20 seconds but nanoparticles with a core diameter of 26nm will keep the information (magnetic orientation) for more than 800 years.

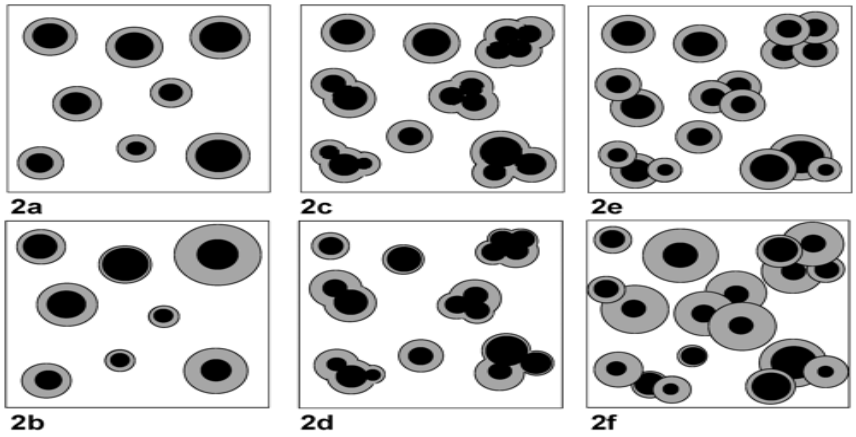

Figure 31: possible particle distribution, (2a) the size of magnetic cores can differ, whilst the thickness of the coating remains the same. (2b) size of individual particles can be constant, thickness differing. (2C) some of the individual particles agglomerated i.e. stable agglomerates with constant thickness. (2d) of variable thickness of the polymeric coating. The particle size may also vary due to the agglomeration of coated nanoparticles (2e, 2f). (C Gross et al)

As, can be seen from figure 30 during chemical synthesis the nanoparticles can produce quite a broad particle size distribution. This can be due to the variation in the core diameter of the particles, the thickness of the coatings or even different stages of agglomeration.

From, this it can be seen why it is important to find the nanoparticles size. There have been different methods that have been discussed in literature most popular being Magnetic Fractionation followed by the photon correlation spectroscopy.

Magnetic fractionation is conducted by separation columns that are fixed between the pole shoes of the electromagnet and then rinsed with 2ml of buffer solution (phosphate buffered saline, pH 7.4). Then at a current of 6A, 500µl of the Ferrofluid is added. The column is rinsed with the buffer solution until the elute is clear, this would be the 6A fraction. The field is then reduced and the next elute gathered. This procedure is repeated until no current is applied. The column is then removed from the magnet and the remaining nanoparticles are eluted with buffer solution and gathered. The hydrodynamic diameter of the nanoparticles can be then measured by the PCS (i.e. ZetaSizer) or the particles can be investigated using the Atomic Force Microscope, where the diameter is determined from the height images.

In this instance, the PCS was used to determine the particle size without the conducted magnetic fractionation. The results of this was that instead of each singular particle being measured the liquid was measured as one in a bulk, this can be due to agglomeration of the particles therefore the particles being attracted to one another. Due, to this it was deemed simpler to use the SEM technique to determine an average size of the magnetic core diameters.

The average sizes that were found via the SEM particles are as follows:

Sample	Particle Size (nm)	Average Size (nm)	Agglomeration scale 1-10	Coating Quality Scale 1-10
1)-1,1,1,-1	17.30			
	11.53			
	19.945	**16.289**	**3**	**2**
	20.18			
	12.49			
2) 1,-1,-1,1	28.83			
	24.02			
	19.22	**20.18**	**9**	**7**
	9.61			
	19.22			
3) -1, -1, 1, 1				
4) 1,-1,1,-1	10.57			
	13.46			
	8.65	**11.918**	**7**	**6**
	15.38			
	11.53			
5) 1,1,1,1	11.53			
	13.45			
	16.34	**14.222**	**8**	**7**
	14.41			
	15.38			
6) -1,-1,-1,-1	13.45			

Sample	Particle Size (nm)	Average Size (nm)	Agglomeration scale 1-10	Coating Quality Scale 1-10
	16.34			
	16.34	**15.184**	**5**	**0**
	16.34			
	13.45			
7)-1,1,-1,1	10.57			
	11.53			
	9.61	**10.57**	**2**	**1**
8) 1,1,-1,-1	16.34			
	13.45			
	17.30	**15.93**	**7**	**6**
	16.34			
	19.22			

Key	
1	Poor: high level of agglomeration & poor coating
10	Very Good: Low level of agglomeration & good coating

From this it can be seen that the average size for the magnetite nano-particle is generally between 10 to 16nm in size.

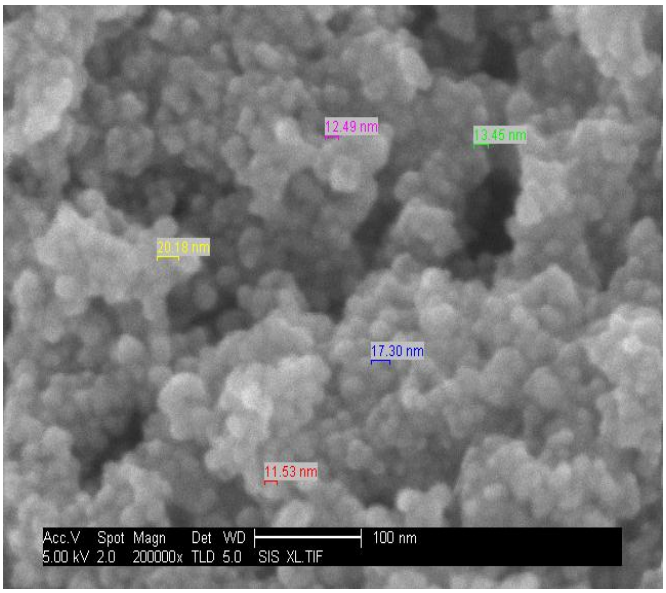

Figure 32: Sample one taken at approx.130 x, agglomeration can be seen as well as the particles.

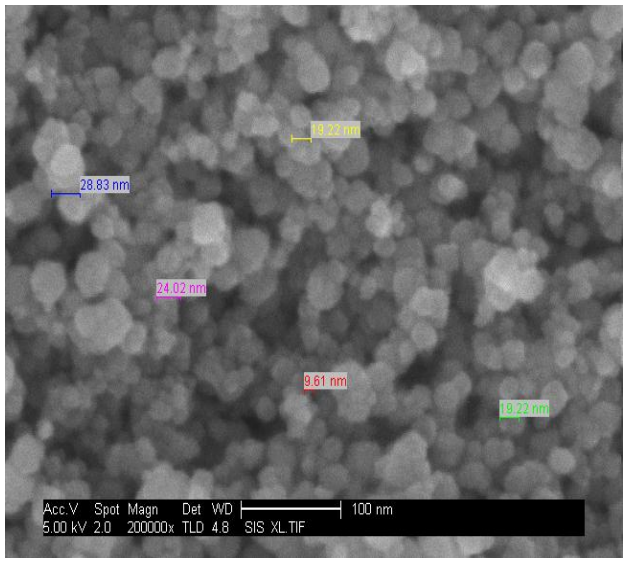

Figure 33: Sample two at a magnification of 200K. The particles in this sample appear to be more clearly defined, with each particle being in its separate entity.

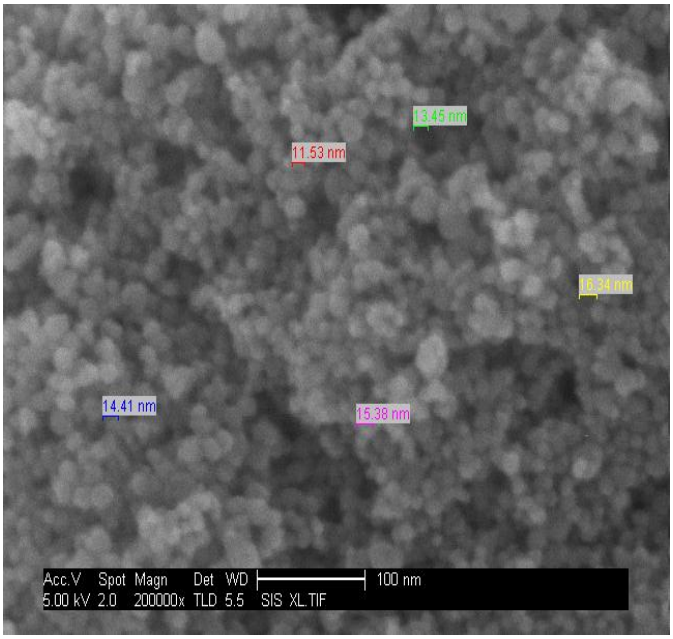

Figure 34: Sample four at a magnification at approx.144x. Very small particles regularly distributed.

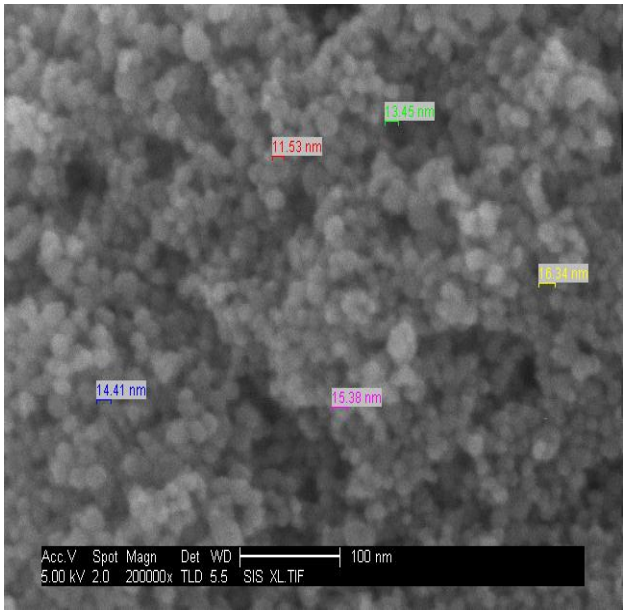

Figure 35: Sample five at a magnification at approx.144x. Little agglomeration observed.

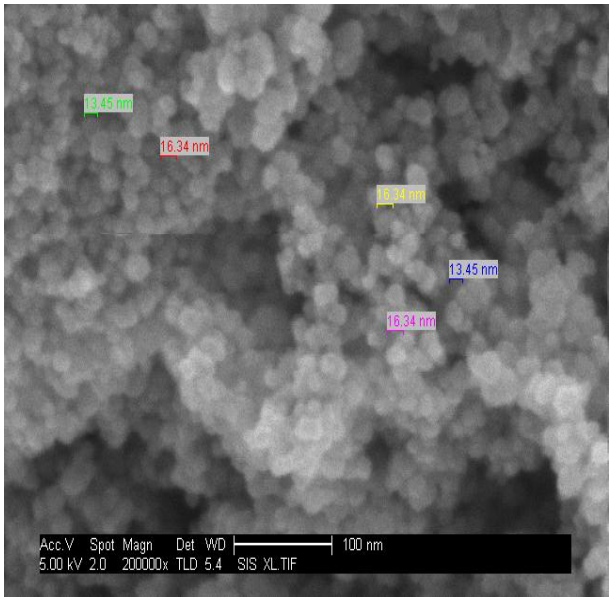

Figure 36: Sample six at a magnification at approx.118x. Agglomeration can be seen in sample.

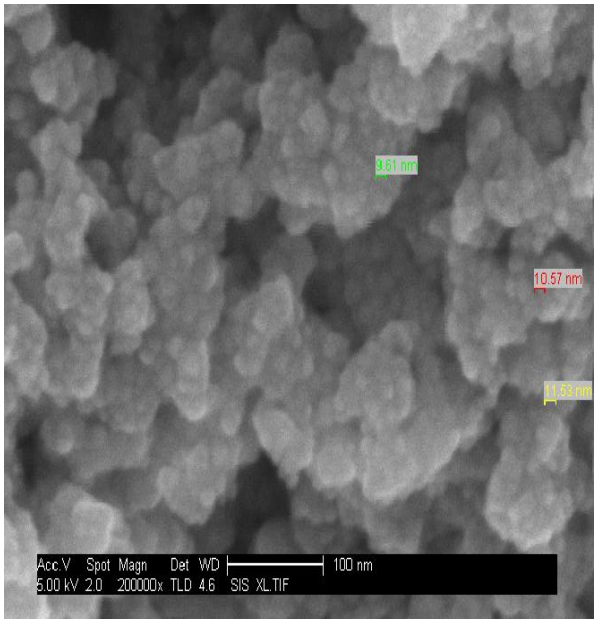

Figure 37: Sample seven at a magnification at approx.118x. Large amount of agglomeration can see groups of particles being clumped together.

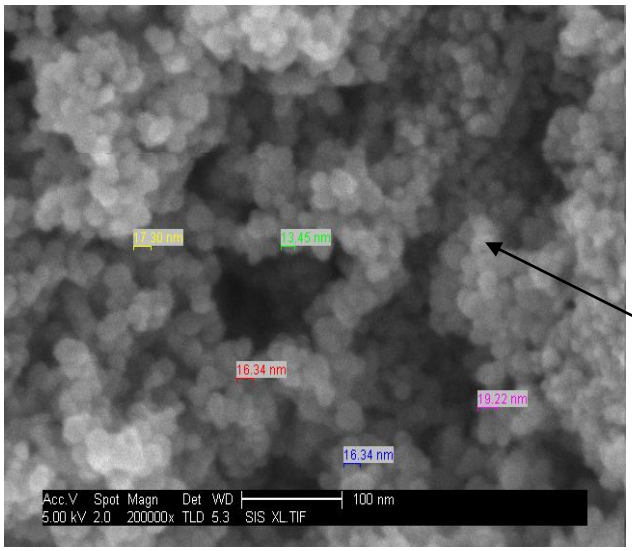

Halo like appearance seen around the particles.

Figure 38: Sample seven at a magnification at approx.144x. Little agglomeration, single particles seen clearly

Figure 32 shows sample one at a magnification of 200K. There are signs of agglomeration, and a soapy kind of coating can be seen clumping the separate particles together, the outline of the different particles can be seen but they appear to be housed together in separate bubbles, coating 5 or 6 at a time. Therefore, concluding, that rather than coat one particle separately, the Oleic Acid appears to coat multiple at a time.

Figure 33 shows sample two at a magnification of 200K. The particles in this sample appear to be more clearly defined, with each particle being in its separate entity. The average size of particle in sample two also appear to be much larger in size compared to sample one. The size of particles within the sample itself appears to be very varied, ranging from 9.61nm to 28.83nm. Therefore, showing that each sample will have varying particle sizes and to obtain a uniform size may not be as simple as it has been assumed.

Figure 34 shows sample four at a magnification of 200K. Here the concentration was higher compared to sample two; this can be attributed to why the particles appear smaller in size. There is very little agglomeration, and the separate particles can be seen. This lack of agglomeration can be attributed to the surfactant Tetramethylammonium Hydroxide being used. From, the three samples that have been seen so far, it is clear to see that when Oleic Acid is used there appears to be much more agglomeration compared to when Tetramethylammonium Hydroxide is used. The particles are also more clearly defined and they can be seen to be thinly coated compared to the “lumpiness” of sample one.

Figure 35 shows sample five at a magnification of 200K. There is very little agglomeration, the particles are much smaller in size but they are very clearly defined.

Figure 36 shows sample six at a magnification of 200K. There is agglomeration present compared to the previous sample and the particles appear to be bigger. This again can be attributed not only to the surfactant but also the time and temperature. As, the fluid was left to stir for 30 minutes rather than 15. It can be seen from this that temperature may not be as important as it was previously assumed. This sample was formulated at 80°C.

Figure 37 shows sample seven at a magnification of 200K. The agglomeration is much greater; this can be attributed to the higher temperature that this sample was made at, with the addition of Oleic Acid. This is due to the Oleic acid being better suited to be a surfactant for oil based Ferrofluid due to the steric repulsions being produced; rather Oleic acid being used in water based ferrofluid.

Figure 38 shows sample eight at a magnification of 200K. The particles appear to be clustered together and very well defined. The outline of the particles can be clearly seen

and the particles appear to be very much smaller in diameter than those that have previously been seen. There also appears to be a bright “halo” like effect on some particles, very clearly showing the coating around the particles.

From the table and sample pictures it is clear to see that the particle sizes tend to vary between 16 to 20nm, which is considerably smaller than the usual norm of approximately 30 to 40nm. The particles that are coated with Oleic acid do have a much greater tendency to agglomerate in clumps where at times it is not very easy or clear to differentiate the different particles. This is not the case with using Tetramethylammonium hydroxide as a surfactant as the particles can be seen to be much more defined compared to their counterparts. From, sample one it can also be seen that the particles are more separate rather than their counterparts and the particle size is slightly bigger at an average size of 17.73nm. This can also mean that the time of leaving the solution to stir has more of an effect rather than the temperature, as the normal temperature that is used is 80ºC, sample one was conducted at 60ºC and it was left to stir longer for 30 minutes rather than 15 minutes.

The characterisation of sample two was not able to be conducted due to a large amount of charging up at the surface. The surface appeared to be non-conductive therefore the sample was building up a charge. Due to this a TEM characterisation was conducted in order to see the particles more clearly and to also try to see the coating around the particle. This is because with the TEM the electron beam is transmitted through the sample rather than the SEM where secondary electrons are detected around the sample due to excitation by the primary electron beam. The TEM also produces a higher level of resolution.

It must also be remembered that a drying process was taken place and the sample was thinned with alcohol before they were characterised. This will also contribute to how the sample is seen, some properties may have been lost and the particles may appear to be smaller and more grouped together due to the drying process. In, order to see the actual properties of the sample it is ideal to characterise the samples in its natural form. This was attempted with the ESEM, but due to the high conductivity of the sample an accurate representation of the sample was not seen. In, the future it would be interesting to characterise the samples via the Wet STEM, as a sample that is in a liquid form and that does have high conductivity is able to be characterised under high vacuum.

In, conclusion it can be seen that the parameters for sample one appears to be the most successful when producing a ferrofluid where the particles appear more uniform and at an

average size of approximately 18 nm. There is also very little agglomeration and the particles appear much defined. Making the factors that were studied in this test to be more desirable.

6.2:TEM Characterisation:

In figure 39 it is clear to see the outline of the surfactant around the nano particle. The surfactant appears to be similar to a "halo" that is transparent around the solid nano particles; the size of the surfactant appears to be an average of approximately 1 to 2 nm. In this image the particles also appear to be more clearly defined rather than having a large amount of agglomeration.

In figure 40 (Sample 2) the image shows there to be more agglomeration compared to the previous image especially at the top of the image. It is easier to see the particles differentiated at the bottom of the image, where the outline of the surfactant can also be seen.

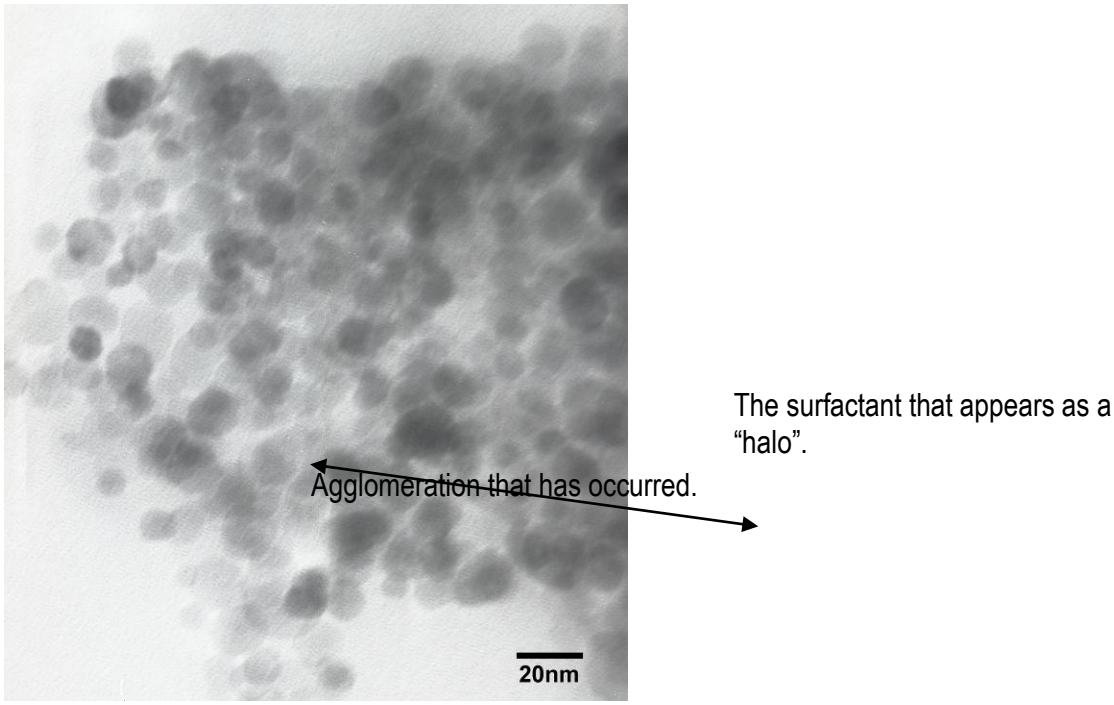

Figure 39, Sample One at a magnification of approx. 305. A halo like appearance can be seen, this can be due to the surfactant or light emitting back from the sample due to characterisation.

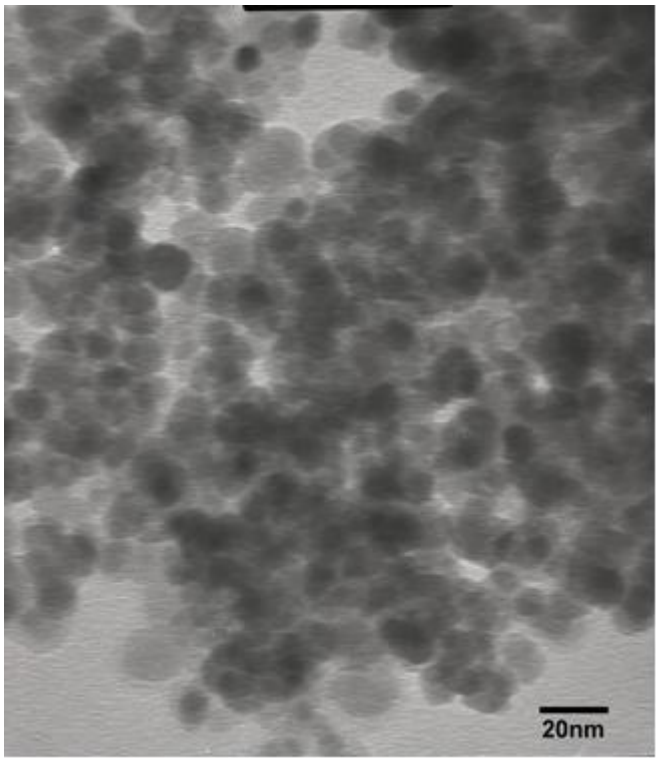

Agglomeration that has occurred.

Figure 40; Sample Two seen at a magnification of approx. 300nm. Agglomeration can be seen in this sample.

6.3: XRD Characterisation:

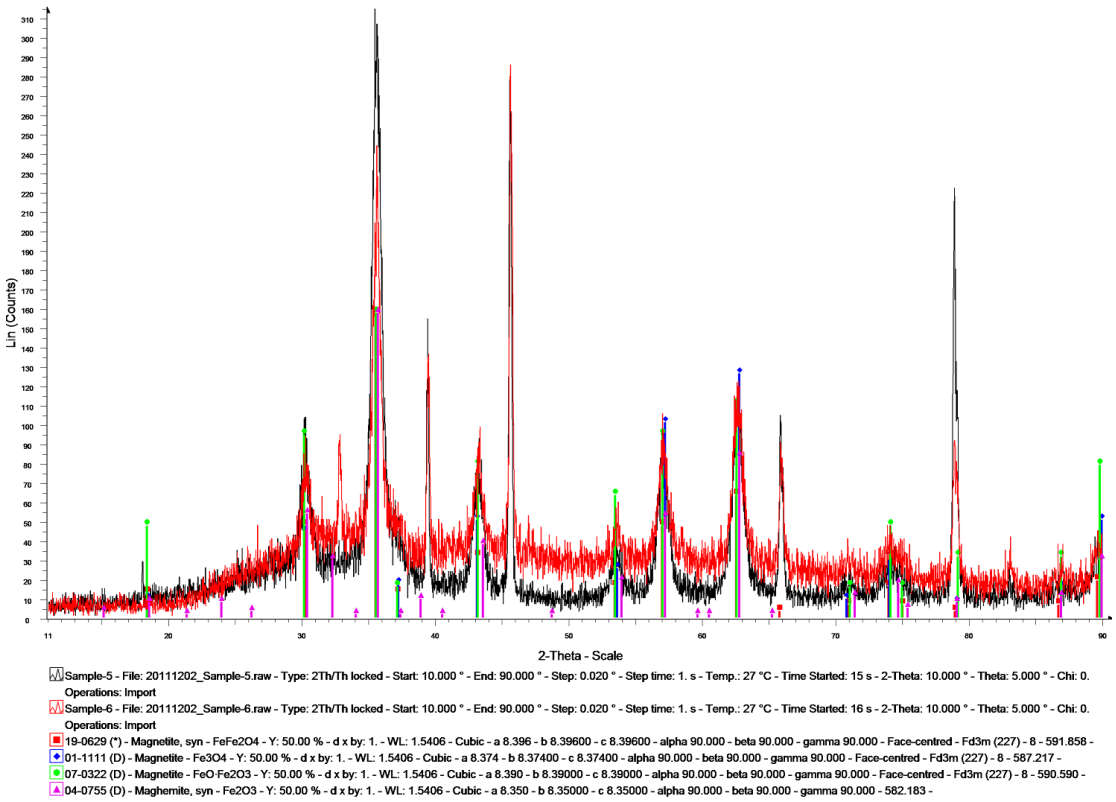

Figure 41: Showing the XRD characterisation of sample five and sample 6.

Samples five and six were respectively characterised due to sample five utilising the surfactant Oleic Acid and sample six Tetramethylammonium Hydroxide. It was clear to see from the XRD samples that despite the tests having different parameters, this did not affect the crystal structure or even the basic structure of the samples. The samples produced a FCC crystal structure and showed that the actual structure that was produced was that of a magnetite with some Maghemite present. This is what it was expected to be. In the XRD characterisation, there does appear to be a peak that is found in sample five that cannot be identified and does appear to be quite high. This is found around the range of: 79 2-Theta. For sample six, there is also a small peak at an approximate of 33 2-Theta, that also appears to be an anomaly. Both of this could be due to the waste salt that is present in the sample that is being characetrised.

6.4: ESEM Characterisation:

Even though it was understood that due to the lack of high resolution and high conductivity it is not ideal to use the ESEM, the ESEM was used as a characterisation method to investigate the elemental composition that was within the structure and where the formations were. From the characterisation, it was found from all of the samples that the pure magnetite was found within the middle of the sample and the waste chlorine and hydrogen was found on the edges of the sample. The amount of chlorine was also found less than what it was assumed to be, where at times in the middle of the sample there would be no chlorine found at all but on the edges majority of the sample would be made up of chlorine. This suggests that the samples seem to have two very different parts. The "waste" part of the solution is dispersed out of the relevant makeup, but is still found within the structure. This is something that is expected, as the actual particle make up when characterised with the XRD showed that majority of the sample was made up from Magnetite and some Maghemite. The presence of waste product was not seen in the actual particle itself.

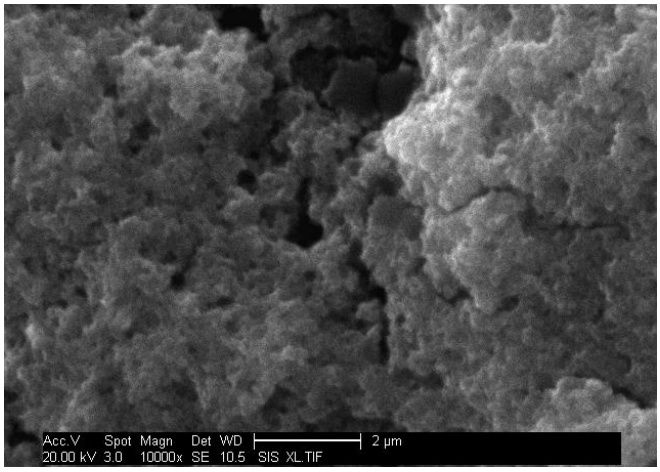

Figure 42: Sample two in the middle of the structure.

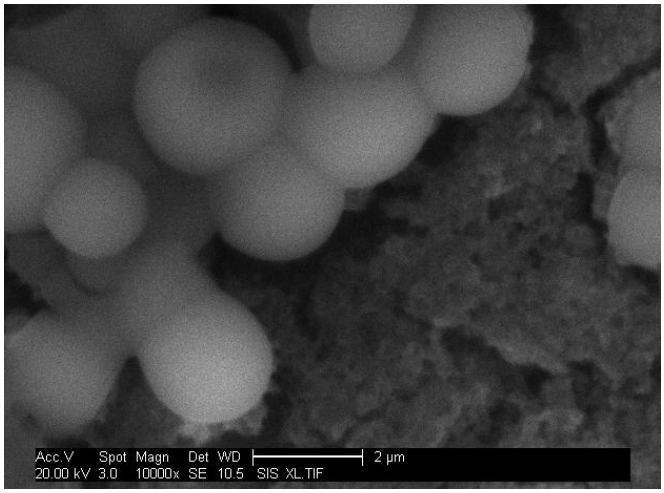

Figure 43: Sample two on the outside of the structure.

7.0: Graphs showing the results from the Statistical Design of Experiments

The experimental design and analysis was carried out using MINTAB software.

Figure 44: The table below shows the design and table of results from the statistical design of experiments

C2	C3	C4	C5	C6	C7	C8	C9	C10	C11
RunOrder	CenterPt	Blocks	Surfact	Temp	Time	Conc	P Size	Agglom	Coat
1	1	1	2	60	15	2	16.289	3	2
2	1	1	1	80	30	1	15.184	9	7
3	1	1	2	80	15	1	*	*	*
4	1	1	1	80	15	2	11.918	7	6
5	1	1	1	60	15	1	15.424	8	7
6	1	1	2	80	30	2	16.914	5	0
7	1	1	2	60	30	1	10.486	2	1
8	1	1	1	60	30	2	17.790	7	6

The above table shows the results that were obtained from the statistical design of experiments, showing both the run order and the results that were obtained from the experiments.

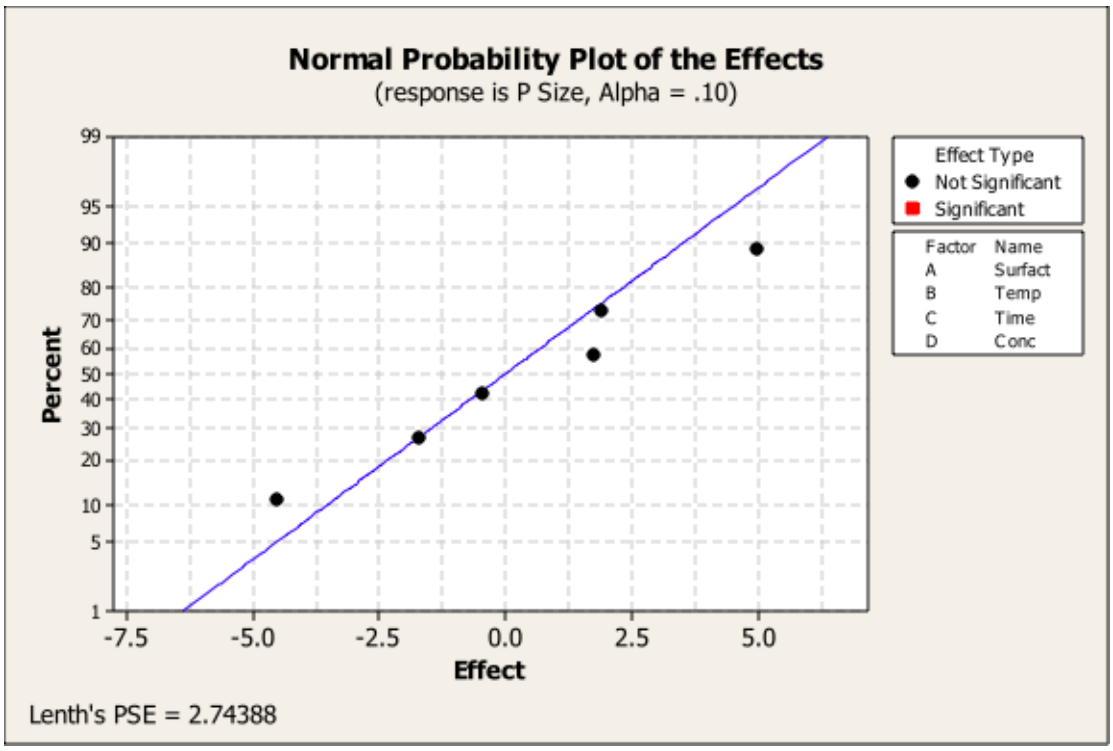

Figure 45: Graph showing the Normal probability plot of the effects.

This plot shows that none of the main factors are singularly significant in explaining the particle size. The level of control was the factors themselves.

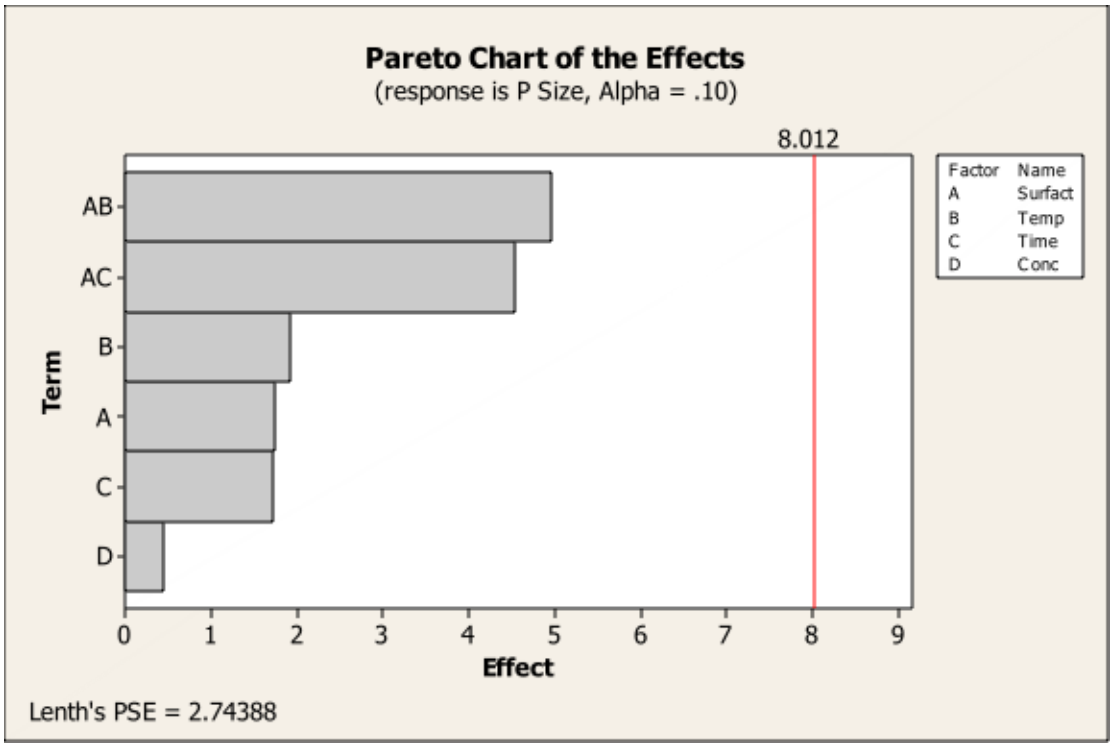

Figure 46: Graph showing the Pareto chart of the effects.

This graph also shows that there is not one singular factor that has been tested that contributes to the particle size. This graph also includes the AB and AC interactions as well as the main factors. So the particle size must be determined by complex interactions between the factors. More interactions would need to be tested in order to explain this, which implies more experimental runs. This was beyond the scope of this work.

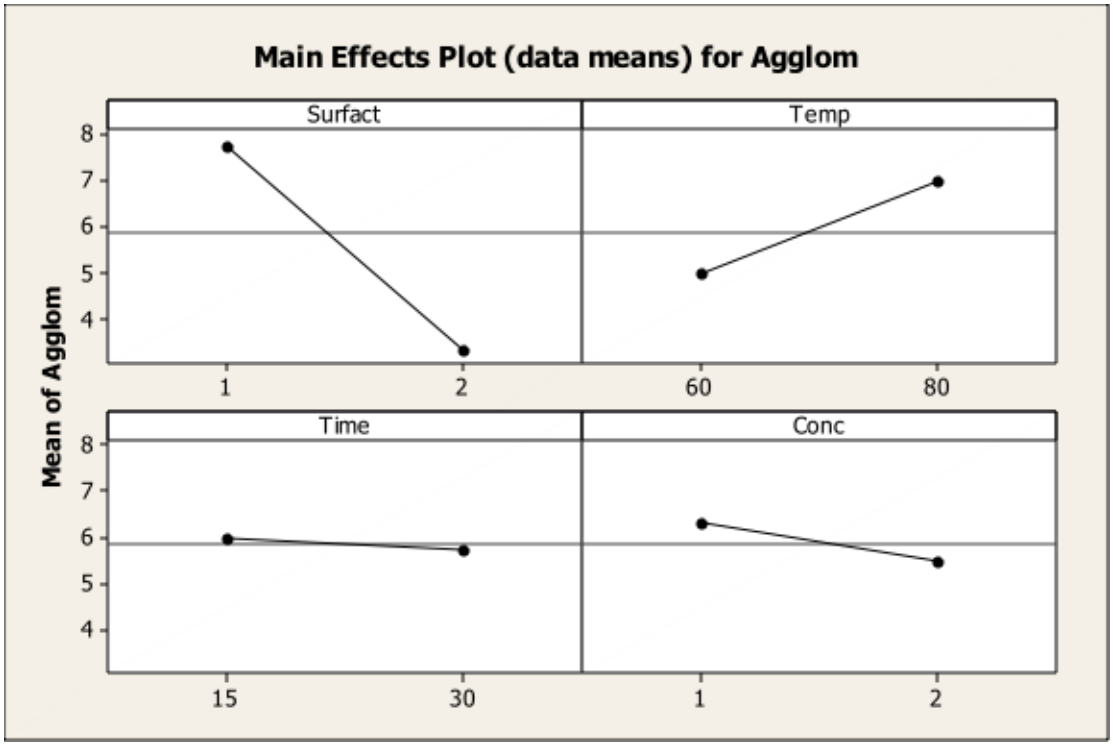

Figure 47: Graph showing the main effects plot (data means) for agglomeration.

In this graph it is clear to see that the surfactant plays a large significant part in the agglomeration of particles when they are formed. This supports the idea that surfactant should be used dependent on if the fluid that is going to be made water based fluid or an oil based fluid. The is also supported by the sample pictures that were taken via the SEM. Samples that were produced with Oleic Acid as a surfactant had a much higher level of agglomeration compared to if Tetramethylammonium Hydroxide was used. This was because the samples that were produced were water based compared to oil based fluids.

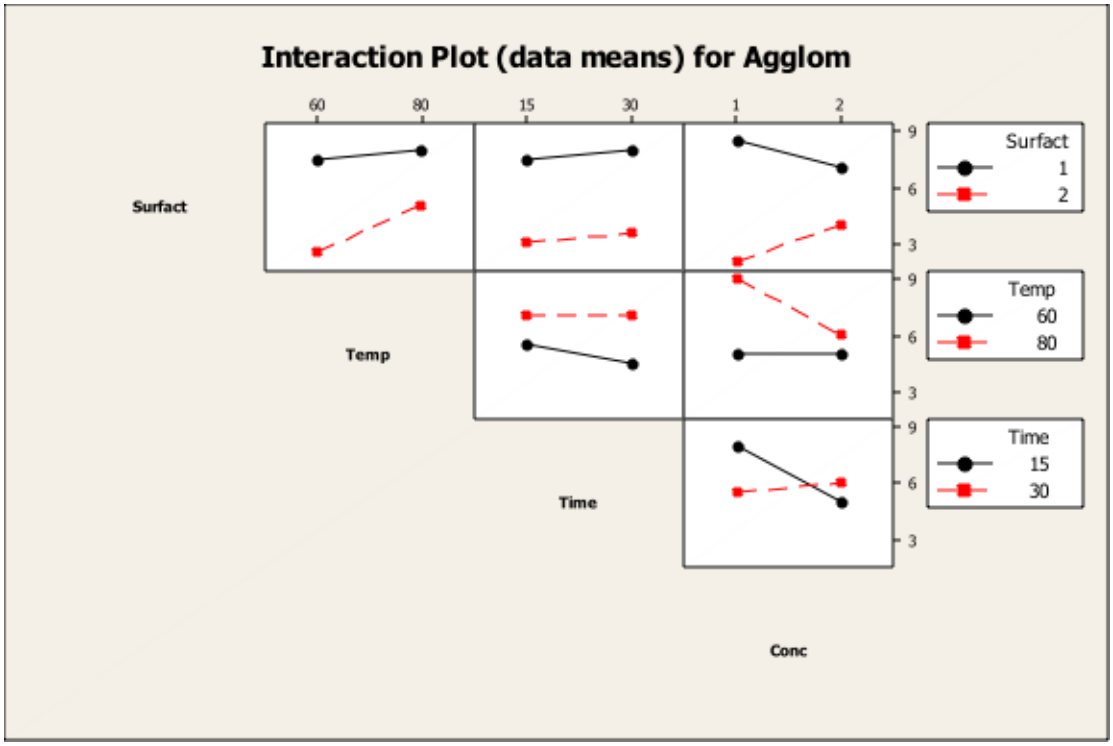

Figure 48: Graph showing the interaction plot (data means) for agglomeration.

This graph clearly shows and supports figure 47, where the surfactant is the main factor for agglomeration to occur in the fluids or not. This is something that was expected as it has been mentioned due to the aquatic nature of the ferrofluid produced Tetramethyl Ammonium Hydroxide will be the best surfactant to use as the level of agglomeration produced is at a reduced level compared to Oleic Acid. Due to the drying method for the preparation of the samples for characterisation of the nanoparticles, there will also be a slight increase in agglomeration. This is something that should also be looked into for further studies. The graph also shows, that time is insignificant for the formation of agglomeration.

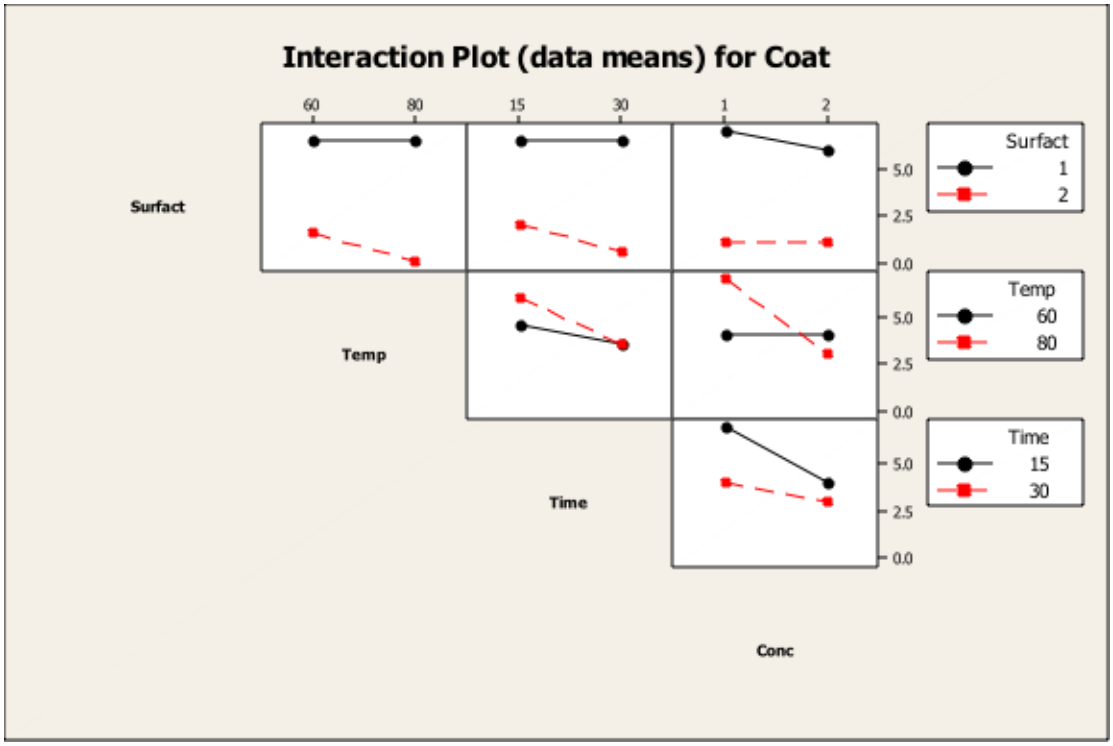

Figure 49: Graph showing the interaction plot (data means) for coat.

The interaction plot for coating again shows that the most significant factor is the surfactant that is used compared to temperature or time. Concentration does not seem to factor at all.

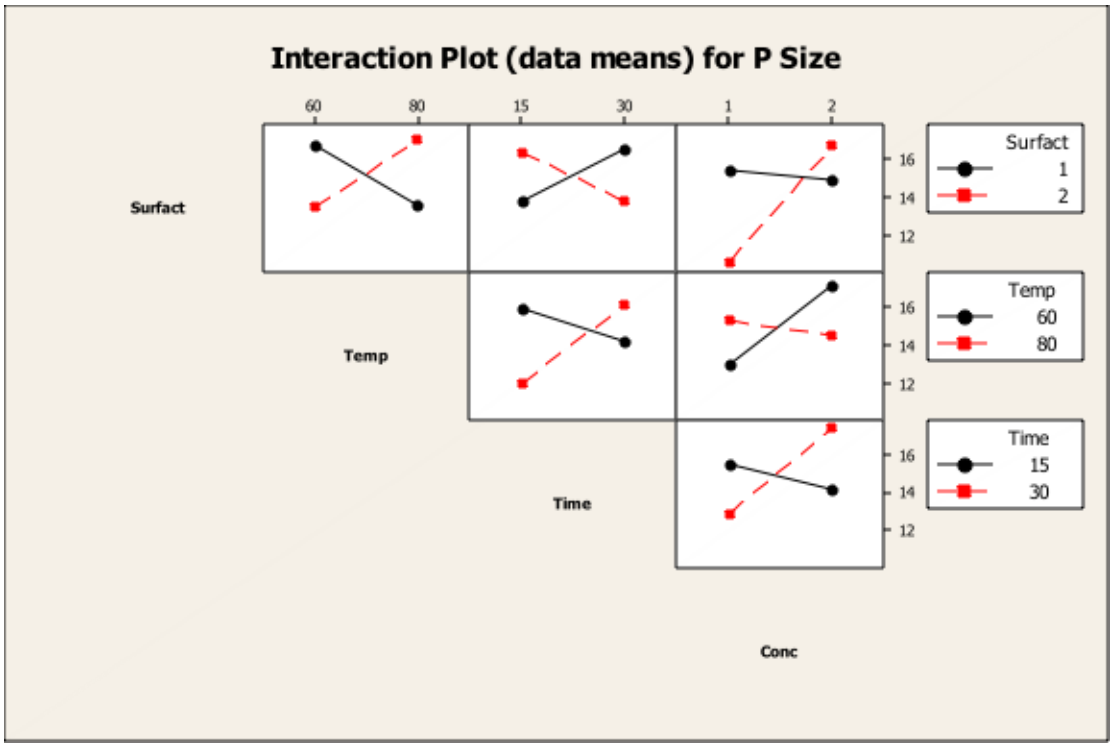

Figure 50: Graph showing the interaction plot (data means) for particle size

The graph for the interaction of particle size is the most significant of all the graphs that were produced. The graphs, based on coating and agglomeration supports the hypothesis stating coating and agglomeration is dependent upon the type of surfactant that is used. In this study we had also hypothesised that the particle size may be dependent upon the temperature or on time. This hypothesis has been disproved and it is seen by the graph. There is not one factor that plays a part in the determination of particle size. The complexity of the set of interactions with the variables is the reason why the particle size cannot be determined. It is not the case where one variable can be changed in order to see what factor the particle size is dependent upon.

Due, to the time dependence of this study an investigation of more runs could not be performed. In, order to find what particle size is dependent upon, more runs do need to be performed as well as looking at a full factorial of all interactions, rather than just some, which as mentioned is beyond this scope of work.

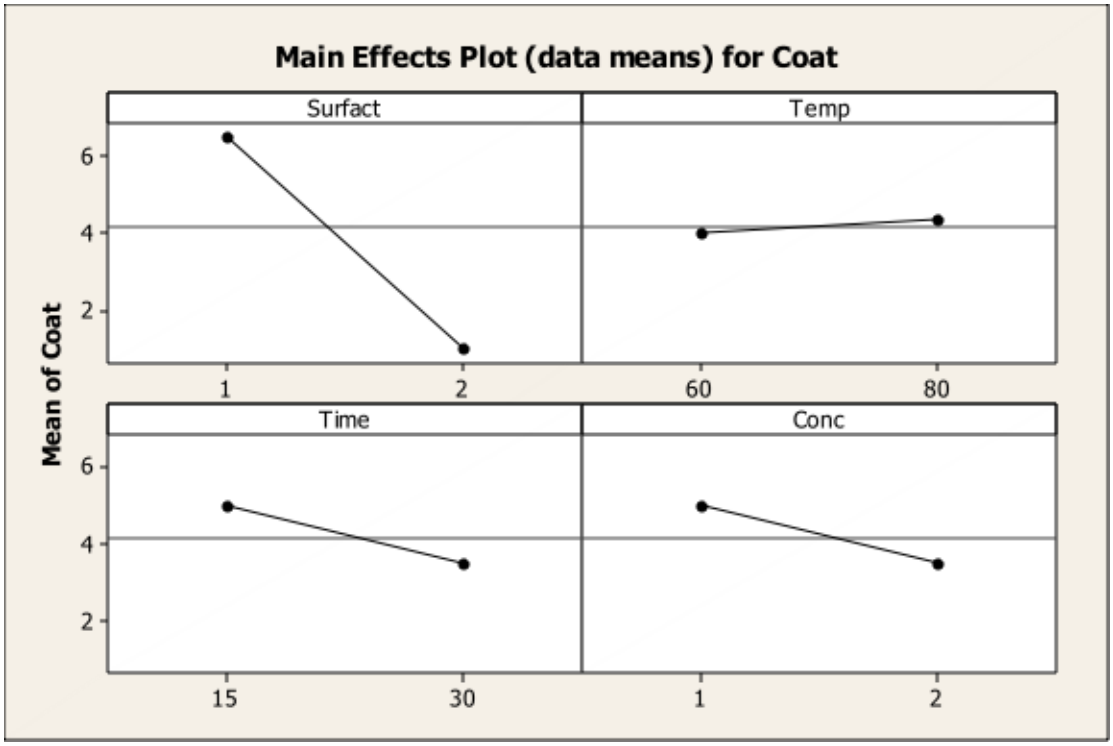

Figure 51: Graph showing the interaction plot (data means) for coating.

From, this graph it can be easily seen that the coating of the particles is very strongly dependent upon the surfactant, hence why there is a big difference in range. The graph also shows that the factor, which has the least to do with the coating, is temperature whilst, time and concentration may play but not a significant part.

8.0: Discussion:

After producing and testing the Ferrofluid with different characterisation methods and different parameters via the statistical tests; it was concluded that test six was the best method that was produced. The surfactant that was used within this test was Tetramethylammonium hydroxide, the temperature the test was conducted at was 60°C, the time 30 minutes and the concentration being one. Tetramethylammonium Hydroxide works best due to the ionic bonding that can occur with the aqueous medium of the ferrofluid; this is due to the surfactant being ionic and producing electrostatic repulsions. It was also found that the temperature when producing the ferrofluid was not as a big factor as it was assumed to be. It was the norm to produce the ferrofluids at a temperature of 80°C rather than 60°C. From the tests that were conducted it can be seen that there was not much of a difference between the two temperatures. The nano particles for the tests that were conducted at 60°C was approximately an average particle size of an approx. 20nm, this was also the same for 80°C. The stirring time of the total percentage of the fluid was also a factor that was concerned but if test 1, 3 and 6 is taken into account as being the top three batch of the fluid; it was only test 6 that had the time to be at 30 minutes rather than 15 minutes, again showing that the time left to stir was not as important as it had appeared to be and a reaction was not generated with the extra time that the solution was left to be stirred. The top three tests have two things that are in common one being the same surfactant, tetramethylammonium hydroxide and the second being the concentration. The concentration of the method that was used was changed very slightly by the concentration of ammonium hydroxide being doubled and the concentration of Iron Chloride solution remaining the same. The effect may occur due to the ammonium hydroxide being a strong base for the ferrofluid and allowing the formation of smaller particles than those that was found before.

From, the XRD that was used it was also shown that the crystals of the magnetite formed a Face Centred Cubic formation, this is what was predicted for the magnetite crystals. This crystallinity is what enables the ferrofluid to be paramagnetic. The magnetism of the ferrofluid is quite obvious as shown in figure 17a and 17b, when a magnet is placed near the fluid, the fluid becomes magnetic and when the magnet is not present the magnetic properties are not obvious.

The small size of the particles also shows that the ferrofluid that was produced also lies in with the theory that the smaller the particles, the more they are able to be suspended within the liquid better. This is due to the high surface area to the volume ratio of the nano

particles within the fluid. The magnetic saturation of the particles also reduces in relation to the particle size increasing in size.

From, the statistical tests and from the graphs that were produced from them. It can be clearly seen that the measurement or understanding how the particle size is formed is much more complex than that was first assumed. From the tests, it showed that none of the factors played a significant role on what determined the particle size; this is clearly seen from graph fifty. It can be clearly seen that more experimental runs are needed, and probably a full factorial DOE, to find out how the particle size is determined. This is beyond the scope of this work but would be interesting for future work.

From the MZ Ferrite that was produced only a small volume had shown magnetic properties this was found by applying magnetic field to the sample. It was also seen from the SEM that the particles were more finely dispersed compared to the Magnetite. In, future work a method needs to be considered were the volume of paramagnetic liquid is of a larger quantity compared to what was produced in this study.

9.0: Conclusion:

After, the different characterisation techniques and conducting the statistical test, it can be concluded, that; in order to produce magnetite that has particle size between the ranges of 15 to 20nm a liquid base would be considered to be better due to the suspension within a liquid base being superior, therefore less agglomeration being produced. It is also important to take into the consideration the surfactant that is being used, as the surfactant is dependent upon the base of the ferrofluid. Water based fluid are suited to Tetramethylammonium hydroxide whereas oil based are more suited to oleic acid. This was apparent during the course of this study as when oleic acid was used as a surfactant for water based ferrofluid there was a greater percentage of agglomeration compared to that of Tetramethylammonium hydroxide. It can also be seen that time has more of an effect whilst making the ferrofluid compared to temperatures that range from sixty to eighty Celsius. In further work, the temperature can be considered again with the samples being produced at a very low temperature of approximately twenty Celsius that is then compared to eighty Celsius. The samples also showed a very strong paramagnetic behaviour with being highly attracted to a magnet being present, and this magnetism thus disappearing with nonmagnetic materials being present and also with one and another.

From, samples that were produced prior to the statistical test it can be seen that reproducing the fluids to be exactly the same is not realistic; this can be seen due to the

lack of reproducibility that was found within the samples that were produced. This is due to the sizes of the nano particles that can vary between different ranges. With, a bulk of fluid being present the small variation between sizes would not make a difference; therefore it can be concluded that if the properties remain the same the reproducibility of the fluid would not create the biggest effect.

It can also be concluded that the crystal structure remains the same even with variations with the parameters.

To conclude, it can be seen that the nano particle of the ferrofluid has an average size of approximately eighteen nanometres, with the surfactant size being approximately one to two nanometres covering the particles thoroughly. Agglomeration decreases dependent on the liquid base and the surfactant being used and hundred per cent reproducibility is not possible, but that should not affect the properties of the fluid. As, mentioned in the discussion in order to find out exactly what affects the particle size more runs would need to take place and also a full factorial DOE, this can be considered for future work. In, this instance it was shown that even with the particles size varying within one sample the properties would not differ greatly. Even, so, this went further than the scope of this work and would be an interesting thread for future work.

10.0: References:

R. Arulmurugan, G. Vaidyanathan, S. Sendhilnathan, B. Jeyadevan, (2006), Mn-Zn Ferrite nanoparticles for ferrofluid preparation: Study on thermal-magnetic properties.. Journal of Magnetism and Magnetic Materials 83-94

Auzans, E, Zins, D. Blums, E. and Massart, (1999), R. Synthesis and Properties of Mn-Zn ferrite ferrofluids, Journal of Material Science. 34, 1253-1260.

Patricia Berger, Nicholas B. Adelman, Katie J. Beckman, Dean J. Campbell, Arthur B. Ellis, George C. Lisensky, (1999), Preparation and Properties of an Aqueous Ferrofluid, Journal of Chemical Education , Vol 76 No. 7

Bica, D., Vekas. L, and Rasa, M. Preparation and magnetic properties of concentrated magnetic fluids on alcohol and water carrier liquids. Journal of Magnetism and Magnetic Materials. 252, 10-12.2002.

A.Bogner, G. Thollet, D.Basset, P.-H. Jouneau, C. Gauthier, (2005), Wet-STEM: A new development in environmental SEM for imaging nano-objects included in a liquid phase, Ultramicroscopy; 104, 290-301.

A.Bogner, P.-H. Jouneau, G. Thollet, D.Basset, C. Gauthier, (2007), A history of scaning electron microscopy developments: Towards “wet-STEM” imaging. Micron; 38, 390-401.

Box, G.E.; Hunter, J.S., Hunter,W.G. (2005). Statistics for Experimenters: Design, Innovation, and Discovery, 2nd Edition. Wiley.

Buschow, K.H.J. and De Bower, F.R. (2003), Physics of Magnetism and Magnetic Materials, Springer Science, New York.

Li-Chieh, H. (2006), Device and method for ferrofluid power generator and cooling system. Patent: 7095143, US.

Danilatos. D. G and Robinson, (1979), E. N. V. Principles of Scanning Electron Microscopy at High Specimen Chamber Pressures. Faculty of Applied Science, the University of New South Wales, Australia, Scanning Vol. 2, 72-82

Peter J Goodhew, John Humpherys, Richard Beanland, Electron microscopy and analysis, third edition, pages: 38, 78, 110, 159, 222-4.

Hatton, T. A., Laibinisand P. E. and Shen. L, (1999), Aqueous magnetic fluids stabilized by surfactant bilayers. Journal of Magnetism and Magnetic Materials, Volume 194, Issues 1-3, 37-44.

S.E.Khalafallam G.W Reimers and George. W, (1980), Preparation of dilution-stable aqueous magnetic fluids. Volume MAG-16, Issue 2, 178-183

M.H.Loretto, Electron beam analysis of materials, second edition, Champan and Hull.

Love, L. J.; Jansen, J. F;Mcknight, T.E; Roh, Y. and Phelps, T. J, (2004), A magnetocaloric pump for microfluidic applications, IEEE transactions on nanobioscience, vol 3, n 2.

Juan Esteban Catano Montoya, Development of a magnetocaloric pump for applications in heat pipes, university of Puerto Rico.

Shirley A Muller, Ueli Aebi and Andreas Engel, What transmission electron microscopes can visualize now and in the future.

Odenbach, S (2002), Ferrofluids, Magnetically Controllable Fluids and their applications, Springer – verlag, Berlin.

Odenbach, S (2003), Ferrofluids- Magnetically controlled suspensiohns, colloids and surfaces A: Physiochemical and Engineering Aspects, Vol 217, NO's 1-3, p171-178.

Odenbach S, (2006), Ferrofluids in Buschow K ed. 2006. Handbook of Magnetic Materials, Vol 16. Amsterdam, Elsevier. 153.

Popplewell, J. Al-Qenaie, A. Charles, S. W. Moskowitz, R. Raj, K, (1982) Thermal Conductivity Measurements on Ferrofluids, Colloid and Polymer Science , Vol 260, No 3, 333-338
Rosensweig, R.E. (1985), Ferrohydrodynamics, Cambridge University Press, Cambridge.

Schmidl, F., Weber, P., Koettig, T., Buettner, M. Prass, S., Becker, C., Mans, M. Heinrich, J. Roeder, M. Wagner, K. Berkov, D.V. Goernert, P. Gloeckl, G. Weitschies, W, and Seidel,P, (2007), Characetrisation of energy barrier and particle size distribution of lyophilized ferrofluids by magnetic relaxation measurements. Journal of Magnetism and Magnetic Materials, 311, 171-175.

Lifen Shen, Paul E. Laibinis, and T. Alan Hatton, (1998). Bilayer Surfactant Stabilized Magnetic Fluids: Synthesis and Interactions at Interfaces, Department of Chemical Engineering, Massachusetts Institute of Technology, Langmuir 15, 447-453

Shimoiizaka, J., Nakatsuka, K., Fujita, T. and Kounosu, A. 1980. Sink-float separators using permanent magnets and water based magnetic fluid. IEEE Trans. Magnetics M-A-G-16 (2), 367-71.

Tishin, A. M. and Spichkin, Y. I. (2003), The Magnetocaloric Effect and its Applications, Taylor and Francis Ltd, London.

Vekas, L, Rasa, M. and Bica, (2000), D. Physical properties of magnetic fluids and nanoparticles from magnetic and magneto-rheological measurements. Journal of Colloid and Interface Science. 231, 247-254.

Shigang Wang, Handan Liu and Wei Xu. (2008) Hydrodynamic modelling and CFD simulation of ferrofluids flow in magnetic targeting drug delivery. Journal: International Journal of Computational Fluid Dynamics. Vol. 22, No. 10, 659-667

Anthony Wooding, Melvyn Kilner and David B Lambrick, (1988), Studies of the double surfactant layer stabilization of water based magnetic fluids. Journal of Colloid and Interface Science, Volume 144, Issue 1, pages 236-242

Zheng ZG, Zhong. C, Zhang YH, Yu HY, Zeng D.C, (2008), Synthesis, Structure and magnetic properties of nanocrystalline ZnxMn1-xFe2O4 prepared by ball milling. Journal of Alloys and compound V 66 pp. 377-382.

Zimmermann. K, Zeidis. I, Bohm. V and Popp. J, (2009), A contribution about ferrofluid based flow manipulation and locomotion systems. Journal of Physics, V 149 conference series.

Zins, D., Cabuil, V. and Massart, R, (1999), New aqueous magnetic fluids. Journal of Molecular Liquids. 83, 217-232.

Maity. D, Agrawal. C. D. (2007), Synthesis of iron oxide nanoparticles under oxidizing environment and their stabilization in aqueous and non-aqueous media. Journal of Magnetisation and Magnetic Materials 308, 46-55.

Qiang Li, Yimin Xuan, (2009), Experimental Investigation on heat transfer characteristics of magnetic fluid flow around a fine wire under the influence of an external magnetic field. Experimental Thermal and Fluid Science, 33, 591-596

Bruce.M. Moskowitz, (1991), Hitchiker's guide to magnetism. Institute for Rock Magnetism

J.L. Viota, J.D.G. Durán, F. González-Caballero, A.V.Delgad, (2007), Magnetic properties of extremely bimodal magnetite suspensions. Journal of Magnetism and Magnetic Materials. Volume 314, Issue 2, 80-86

Poddar, P, Srikanth, H., Morrison S.A, Carpenter, E E. E. (2005) Inter-particle interactions and magnetism in manganese - zinc ferrite nanoparticles. Journal of Magnetism and and Magnetic Materials, 288, 443-451.

http://www.uhh.hawaii.edu/~kenhon/mineralogy/lab-syllabus/xtal-xray/XRDmethod.html